RESEARCH ARTICLE

BCOR and *BCORL1* Mutations Drive Epigenetic Reprogramming and Oncogenic Signaling by Unlinking PRC1.1 from Target Genes

Eva J. Schaefer[1], Helen C. Wang[1], Hannah Q. Karp[1], Clifford A. Meyer[2], Paloma Cejas[3], Micah D. Gearhart[4], Emmalee R. Adelman[5,6], Iman Fares[1], Annie Apffel[7], Klothilda Lim[3], Yingtian Xie[3], Christopher J. Gibson[1], Monica Schenone[7], H. Moses Murdock[1], Eunice S. Wang[8], Lukasz P. Gondek[9], Martin P. Carroll[10], Rahul S. Vedula[1], Eric S. Winer[1], Jacqueline S. Garcia[1], Richard M. Stone[1], Marlise R. Luskin[1], Steven A. Carr[7], Henry W. Long[3], Vivian J. Bardwell[4], Maria E. Figueroa[5], and R. Coleman Lindsley[1]

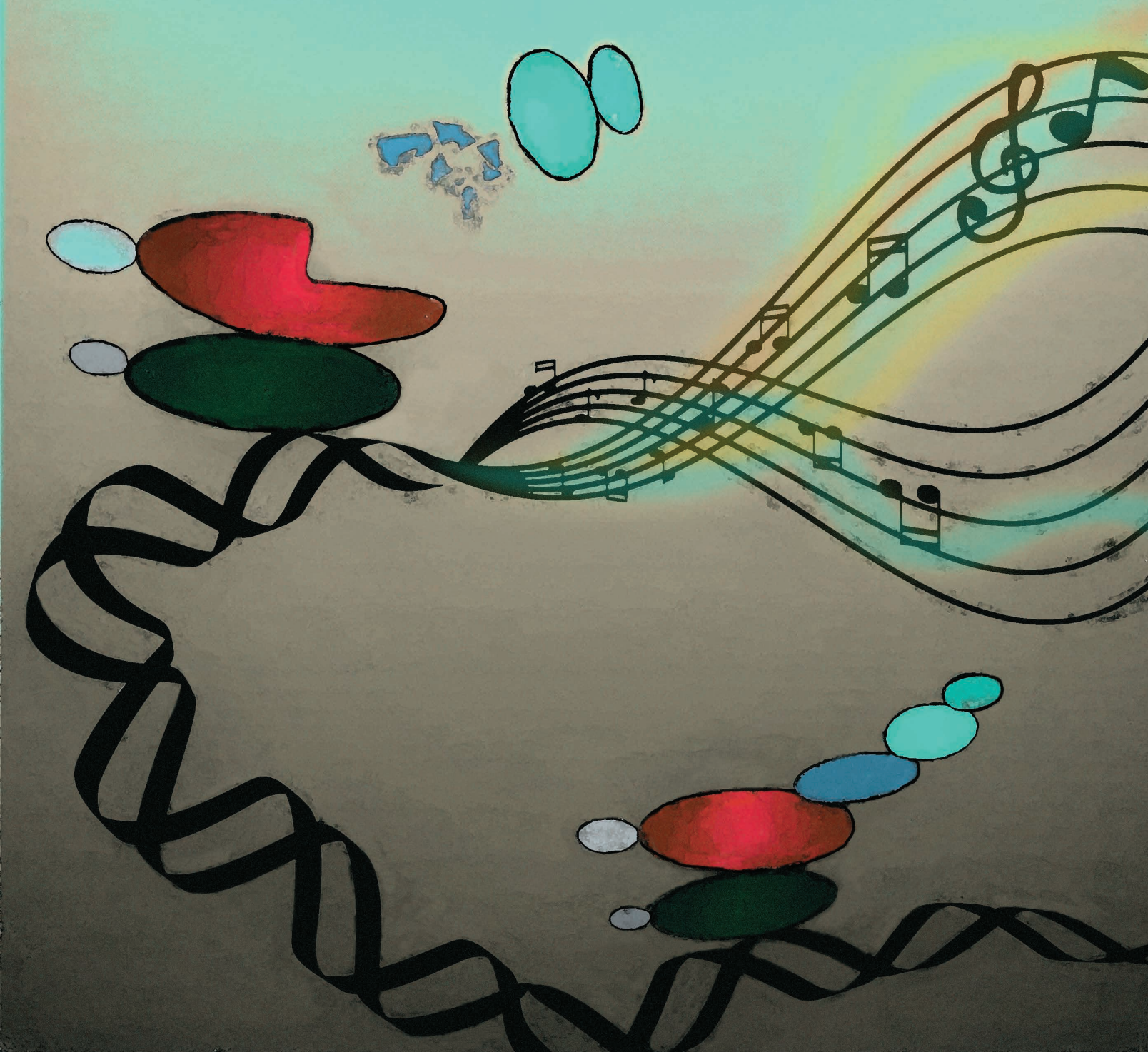

ABSTRACT Polycomb repressive epigenetic complexes are recurrently dysregulated in cancer. Unlike polycomb repressive complex 2 (PRC2), the role of PRC1 in oncogenesis and therapy resistance is not well-defined. Here, we demonstrate that highly recurrent mutations of the PRC1 subunits *BCOR* and *BCORL1* in leukemia disrupt assembly of a noncanonical PRC1.1 complex, thereby selectively unlinking the RING-PCGF enzymatic core from the chromatin-targeting auxiliary subcomplex. As a result, *BCOR*-mutated PRC1.1 is localized to chromatin but lacks repressive activity, leading to epigenetic reprogramming and transcriptional activation at target loci. We define a set of functional targets that drive aberrant oncogenic signaling programs in PRC1.1-mutated cells and primary patient samples. Activation of these PRC1.1 targets in *BCOR*-mutated cells confers acquired resistance to treatment while sensitizing to targeted kinase inhibition. Our study thus reveals a novel epigenetic mechanism that explains PRC1.1 tumor-suppressive activity and identifies a therapeutic strategy in PRC1.1-mutated cancer.

SIGNIFICANCE: We demonstrate that *BCOR* and *BCORL1* mutations in leukemia unlink PRC1.1 repressive function from target genes, resulting in epigenetic reprogramming and activation of aberrant cell signaling programs that mediate treatment resistance. Our study provides mechanistic insights into the pathogenesis of PRC1.1-mutated leukemia that inform novel therapeutic approaches.

INTRODUCTION

Epigenetic pathways are frequently dysregulated in cancer. Somatic gene mutations that alter the repressive function of polycomb repressive complex 2 (PRC2) have been closely linked to the pathogenesis of somatic tumors and hematologic malignancies and can lead to selective therapeutic vulnerabilities (1). In contrast, the tumor-suppressive function of PRC1 and the therapeutic implications of recurrent PRC1 mutations are not well understood.

PRC1 ubiquitylates histone H2A lysine 119 (H2AK119ub) and is a central regulator of cell fate decisions and maintenance of stem cell identity. PRC1 assembles as six different complexes (PRC1.1–PRC1.6), each defined by a specific PCGF linker protein that couples the RING1/RNF2 ubiquitin ligase enzymes to a distinct set of auxiliary subunits (2–4). Among these six PRC1 subcomplexes, PRC1.1 is the most frequently mutated across solid and hematologic cancers. PRC1.1 alterations most commonly involve *BCOR* and *BCORL1*, and these genes are reported to be mutated in 5% to 10% of patients with acute myeloid leukemia (AML) and are associated with poor clinical outcomes (5–12). In chronic myeloid leukemia (CML), which is driven by the BCR–ABL fusion oncogene, *BCOR* mutations have been linked to advanced disease and clinical resistance to BCR–ABL-targeted inhibitors (10).

The impact of PRC1.1 mutations on *in vivo* complex assembly, chromatin localization, and target gene regulation is not understood. As a result, it is not known whether inactivation of the enzymatic function of PRC1.1 is the central driver of PRC1.1 tumors or whether other functions of the complex, such as those mediated by BCL6-binding or AF9-binding domains (13–15), could mediate effects on noncanonical PRC1.1 functions that are independent of H2A ubiquitination activity.

In this study, we analyzed primary AML samples and found that PRC1.1 was affected by highly recurrent *BCOR* and *BCORL1* mutations that truncate the C-terminal PUFD domain. We show that this domain is absolutely required for PRC1.1 complex assembly by linking the RING-PCGF enzymatic core to the chromatin-targeting auxiliary complex, and that enzymatic activity is in turn required for target gene repression in leukemia. We provide a direct mechanistic link between epigenetic reprogramming and activation of oncogenic signaling pathways that mediate disease progression and acquired resistance, pointing the way for

[1]Department of Medical Oncology, Division of Hematologic Neoplasia, Dana-Farber Cancer Institute, Boston, Massachusetts. [2]Department of Data Science, Dana-Farber Cancer Institute, and Department of Biostatistics, Harvard T.H. Chan School of Public Health, Boston, Massachusetts. [3]Center for Functional Cancer Epigenetics, Dana-Farber Cancer Institute, Boston, Massachusetts. [4]Developmental Biology Center, Masonic Cancer Center, and Department of Genetics, Cell Biology, and Development, University of Minnesota, Minneapolis, Minnesota. [5]Sylvester Comprehensive Cancer Center, Department of Human Genetics, University of Miami, Miller School of Medicine, Miami, Florida. [6]Department of Biochemistry and Molecular Biology, University of Miami, Miller School of Medicine, Miami, Florida. [7]Broad Institute of Harvard and MIT, Cambridge, Massachusetts. [8]Department of Medicine, Roswell Park Comprehensive Cancer Center, Buffalo, New York. [9]Division of Molecular Pathology, Department of Pathology, Johns Hopkins University, Baltimore, Maryland. [10]Department of Medicine, Perelman Cancer Center, University of Pennsylvania, Philadelphia, Pennsylvania.

Note: Supplementary data for this article are available at Blood Cancer Discovery Online (https://bloodcancerdiscov.aacrjournals.org/).

Corresponding Author: R. Coleman Lindsley, Department of Medical Oncology, Dana-Farber Cancer Institute, 450 Brookline Avenue, Boston, MA 02215. Phone: 617-632-6649; E-mail: coleman_lindsley@dfci.harvard.edu

Blood Cancer Discov 2022;3:116–35

doi: 10.1158/2643-3230.BCD-21-0115

development of novel therapeutic approaches in cancers with PRC1.1 alterations.

RESULTS

BCOR and *BCORL1* Mutations Cause C-terminal Protein Truncations and Significantly Co-occur in Myeloid Malignancies

To define the frequency and spectrum of PRC1.1 mutations in AML, we performed targeted sequencing of genes encoding all nine PRC1.1 subunits in bone marrow samples from 433 patients with AML. *BCOR* (26/433, 6%) and *BCORL1* (8/433, 1.8%), but not PRC1.1-specific accessory subunits (*PCGF1*, *KDM2B*, *SKP1*, *USP7*) or the pan-PRC1 enzymatic core (*RYBP*, *RING1*, *RNF2*), were recurrently mutated (Fig. 1A; Supplementary Table S1). These genetic findings indicate that selective alteration of PRC1.1 by *BCOR* and *BCORL1* mutations, but not alteration of PRC1 more globally, contributes to the pathogenesis of myeloid malignancies.

In a separate cohort of 3,955 consecutive patients diagnosed with myeloid malignancies, we found that *BCOR* and *BCORL1* mutations were most common in AML (121/1,551, 7.8%) and less common in chronic myeloid neoplasms such as myelodysplastic syndrome (MDS; 36/942, 5.0%), MDS/myeloproliferative neoplasm (MPN;10/343, 2.9%), Philadelphia chromosome–negative MPN (Ph^- MPN; 8/868, 0.9%), and chronic-phase CML (2/251, 0.8%; Fig. 1B). *BCOR* and *BCORL1* mutations significantly co-occurred in both MDS (LR = 4.19, $q < 0.001$) and AML (LR = 3.57, $q < 0.0001$), indicating that they may have cooperative effects in disease pathogenesis (Fig. 1C). Consistent with this hypothesis, analysis of serial samples from individual patients showed that *BCORL1* mutations arose subclonally to preexisting *BCOR* mutations (Fig. 1D; Supplementary Table S2).

In line with previous studies (5, 7, 8, 16), somatic *BCOR* and *BCORL1* mutations most commonly resulted in the introduction of premature termination codons (Supplementary Table S3). Most such nonsense/frameshift mutations (90.8%, 423/466) were predicted to cause reduced protein expression via nonsense-mediated mRNA decay (NMD-sensitive mutations, NMD^+), while 9.2% (43/466) were predicted to cause stable expression of C-terminally truncated proteins lacking the PCGF1-binding PUFD domain (NMD-insensitive mutations, NMD^-; Fig. 1E). Consistent with predictions, we detected expression of a PUFD-truncated BCOR protein in primary AML blasts harboring an NMD-insensitive mutation (Pt.5 BCOR p.L1647fs*3), whereas BCOR protein level was markedly reduced in a primary AML blasts harboring an NMD-sensitive mutation (Pt.3 BCOR p.S1439fs*44; Fig. 1F). Disease-associated *BCOR* mutations thus result in either loss of protein expression or expression of C-terminal truncated protein that lacks an intact PUFD domain.

BCOR and *BCORL1* Mutations Uncouple the PRC1.1 Enzymatic Core from KDM2B

To study the impact of *BCOR*/*BCORL1* mutations on PRC1.1 complex biology, we generated isogenic K562 cell lines with frameshift *BCOR* and/or *BCORL1* mutations that resembled the spectrum of mutations that we observed in patients with myeloid malignancies (Fig. 2A). Predicted NMD-sensitive *BCOR* (exons 7, 9, and 10) and *BCORL1* (exon 8 and 9) mutations resulted in loss of protein expression ($BCOR^{KO}$ and $BCORL1^{KO}$), whereas predicted NMD-insensitive *BCOR* mutations in exon 14 resulted in expression of a C-terminal truncated protein ($BCOR^{PUFD\text{-}Tr}$; Fig. 2B and C; Supplementary Fig. S1A–S1D).

We first used KDM2B-co-IP to define the effect of *BCOR*/*BCORL1* mutations on PRC1.1 complex assembly. In $BCOR^{WT}$/$BCORL1^{WT}$ cells, KDM2B interacted with PRC1.1-defining (BCOR, BCORL1, PCGF1) and accessory subunits (USP7 and SKP1) and pan-PRC1 enzymatic core subunits (RING1/RNF2, RYBP, and CBX8; Fig. 2B). Concurrent disruption of BCOR and BCORL1 resulted in complete uncoupling of the PRC1 enzymatic core from KDM2B, reflected by loss of RING1, RNF2, RYBP, and CBX8 binding (Fig. 2B). This finding was identical in cells lacking BCOR protein expression ($BCOR^{KO}$/$BCORL1^{KO}$) and cells expressing the PUFD-truncated BCOR ($BCOR^{PUFD\text{-}Tr}$/$BCORL1^{KO}$). Together, these results indicate that *BCOR* mutations that are observed in human leukemia, including NMD^+ ($BCOR^{KO}$) and NMD^- ($BCOR^{PUFD\text{-}Tr}$) mutations, have a common effect in PRC1.1 assembly and that BCOR and BCORL1 are essential to couple the PRC1.1 enzymatic core to chromatin-targeting subunit KDM2B.

BCOR–PRC1.1 and BCORL1–PRC1.1 Are Independent Complexes

To determine the distinct contribution of BCOR and BCORL1 to PRC1.1 complex assembly, we performed co-IP analysis in single *BCOR*-mutant cells (Fig. 2C). In KDM2B- and BCORL1-co-IP, we observed preserved KDM2B–BCORL1 interactions with the enzymatic core, indicating that BCORL1 was sufficient to form an intact BCORL1–PRC1.1 complex in the absence of BCOR. Similarly, assembly of a BCOR–PRC1.1 complex was not affected by BCORL1 deficiency (Supplementary Fig. S1D). In wild-type (WT) cells, BCOR and BCORL1 were absent from IP of the reciprocal paralog (Fig. 2C), together indicating that BCOR–PRC1.1 and BCORL1–PRC1.1 complexes assemble independently and are distinct, mutually exclusive species of PRC1.1 *in vivo*.

To quantify the relative contribution of BCOR–PRC1.1 and BCORL1–PRC1.1 to global PRC1.1 levels, we performed BCOR- and BCORL1-co-IP in wild-type (WT) cells and

Figure 1. *BCOR* and *BCORL1* mutations cause C-terminal protein truncations and significantly co-occur in myeloid malignancies. **A,** Frequency of gene mutations in individual PRC1.1 subunits in 433 patients with AML. **B,** Bar plot representing disease distribution of *BCOR* and/or *BCORL1* mutations in 3,955 consecutive patients diagnosed with myeloid malignancies and 1,774 individuals with no hematologic malignancy diagnosis. CML-CP, chronic-phase CML; HM, hematologic malignancy. **C,** Volcano plot representing associations of *BCOR* and *BCORL1* gene mutations in patients with AML (top) or MDS (bottom). The *x*-axis shows the magnitude of association ($\log_2$ OR), and the *y*-axis shows the $-\log_{10}$ *q*-value. **D,** Fish plots representing inferred clonal dynamics based on sequencing. See also Supplementary Table S2. **E,** *BCOR* or *BCORL1* mutations, indicated as NMD sensitive (black; NMD^+) or NMD insensitive (red; NMD^-). Highly conserved regions of BCOR and BCORL1 were determined using Blastp (62). **F,** Western blot analysis (top) of whole-cell lysates from $BCOR^{WT}$- or *BCOR*-mutated AML patient samples. *BCOR* gene expression levels [normalized (norm.) DESeq2 counts, bottom] in $BCOR^{WT}$ or $BCOR^{PUFD\text{-}Tr}$ primary AML patient samples (mean ± SD, $n = 2$ technical duplicates for each condition).

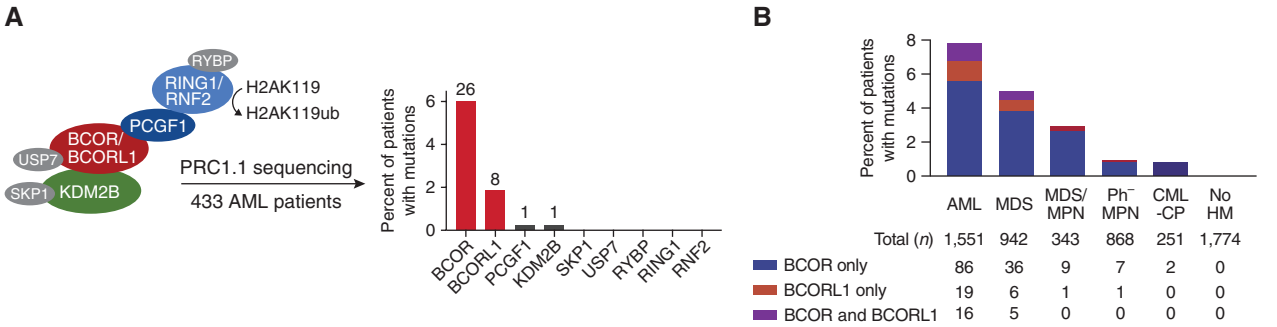
A
RYBP
RING1/
RNF2
H2AK119
H2AK119ub
PCGF1
BCOR/
BCORL1
USP7
SKP1
KDM2B
PRC1.1 sequencing
433 AML patients
Percent of patients with mutations
26
8
1
1
BCOR
BCORL1
PCGF1
KDM2B
SKP1
USP7
RYBP
RING1
RNF2
B
Percent of patients with mutations
AML
MDS
MDS/ MPN
Ph⁻ MPN
CML -CP
No HM
Total (n) 1,551 942 343 868 251 1,774
BCOR only 86 36 9 7 2 0
BCORL1 only 19 6 1 1 0 0
BCOR and BCORL1 16 5 0 0 0 0

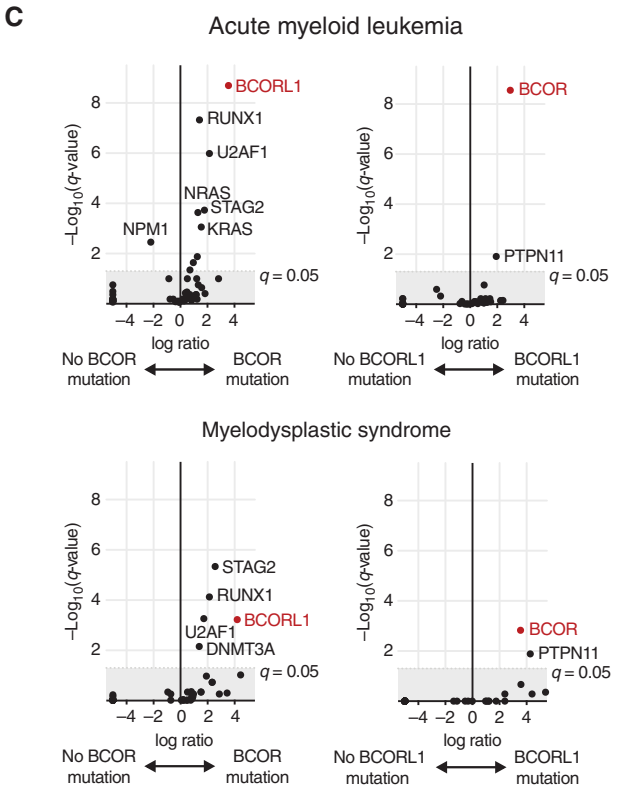
C
Acute myeloid leukemia
BCORL1
RUNX1
U2AF1
NRAS
STAG2
KRAS
NPM1
q = 0.05
log ratio
No BCOR mutation
BCOR mutation
BCOR
PTPN11
No BCORL1 mutation
BCORL1 mutation
Myelodysplastic syndrome
STAG2
RUNX1
BCORL1
U2AF1
DNMT3A

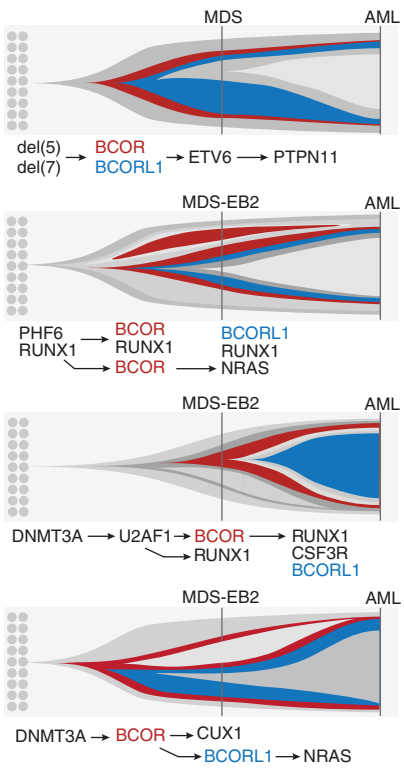
D
MDS
AML
del(5)
del(7)
BCOR
BCORL1
ETV6
PTPN11
MDS-EB2
PHF6
RUNX1
RUNX1
NRAS
DNMT3A
U2AF1
CSF3R
CUX1

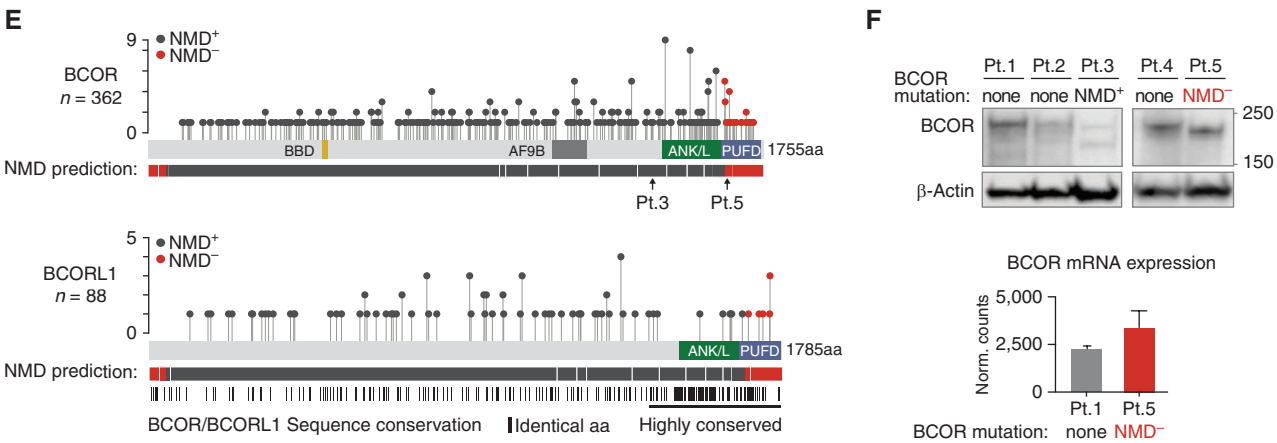
E
NMD+
NMD−
BCOR
n = 362
BBD
AF9B
ANK/L
PUFD
1755aa
NMD prediction:
Pt.3
Pt.5
BCORL1
n = 88
1785aa
BCOR/BCORL1 Sequence conservation
Identical aa
Highly conserved
F
BCOR mutation:
Pt.1
Pt.2
Pt.3
Pt.4
Pt.5
none
none
NMD+
none
NMD−
BCOR
β-Actin
250
150
BCOR mRNA expression
Norm. counts
5,000
2,500
0
Pt.1
Pt.5
BCOR mutation:
none
NMD−

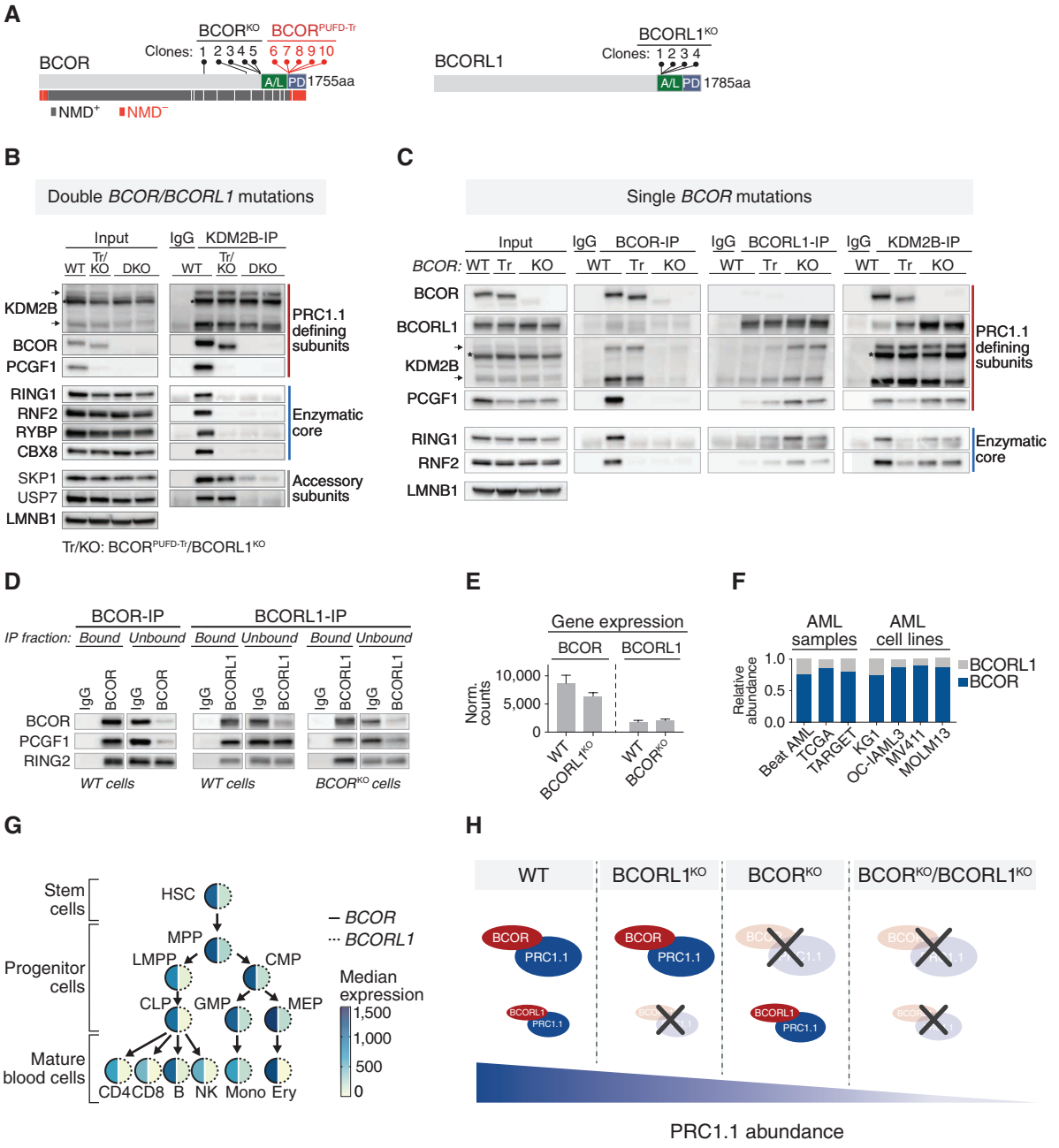

Figure 2. *BCOR* and *BCORL1* mutations uncouple the PRC1.1 enzymatic core from KDM2B. **A,** *BCOR*- and *BCORL1*-mutated cell lines. NMD sensitive (black; NMD^+) and NMD insensitive (red; NMD^-). A/L, ANK/L domains; PD, PUFD domains. **B,** KDM2B-co-IP-Western blot analysis (nuclear extracts) in wild-type (WT), $BCOR^{PUFD\text{-}Tr}/BCORL1^{KO}$ (Tr/KO), or $BCOR^{KO}/BCORL1^{KO}$ (double-knockout, DKO) cells. The DKO clones harbor the same mutations in BCOR (p.P1451fs*) and BCORL1 (p.H1535fs*) and have been derived as independent $BCORL1^{KO}$ clones from the same $BCOR^{KO}$ parent clone. KDM2B-short (90 kDa) and long (152 kDa) isoforms are marked by arrows (asterisk indicates nonspecific band). **C,** BCOR-, BCORL1-, and KDM2B-co-IP-Western blots (nuclear extracts) in WT, $BCOR^{PUFD\text{-}Tr}$ (Tr), or $BCOR^{KO}$ (KO) cells. The $BCOR^{KO}$ clones have been derived as independent clones from WT cells and harbor different BCOR mutations (p.A1453fs* and p.C1080fs*). KDM2B short (90 kDa) and long (152 kDa) isoforms are marked by arrows (asterisk indicates nonspecific band). **D,** Western blot analysis of bound and unbound BCOR- and BCORL1-co-IP fractions in WT or $BCOR^{KO}$ K562 cells. **E,** *BCOR* or *BCORL1* gene expression in the indicated cell lines (mean ± SD). Norm., normalized. **F,** Relative gene expression levels of *BCOR* and *BCORL1* in primary AML samples or AML cell lines as indicated. Fragments Per Kilobase of transcript per Million mapped reads (FPKM) values of AML samples [Beat AML $n = 507$, TARGET $n = 532$, LAML (The Cancer Genome Atlas, TCGA) $n = 156$] were obtained from https://www.cancer.gov/tcga. AML cell line Reads Per Kilobase of transcript per Million mapped reads (RPKM) values are from the Broad Institute Cancer Dependency Map (DepMap Achilles 18Q3 public; available from https://figshare.com/articles/dataset/DepMap_Achilles_18Q3_public/6931364). **G,** Median gene expression of *BCOR* and *BCORL1* in sorted hematopoietic stem/progenitor cells and mature lineages as indicated (63). CLP, common lymphoid progenitor; CMP, common myeloid progenitor; Ery, erythrocyte; HSC, hematopoietic stem cell; GMP, granulocyte-monocyte progenitors; LMPP, lympho-myeloid primed progenitor; MEP, megakaryocyte-erythroid progenitor; Mono, monocyte; MPP, multipotent progenitor; NK, natural killer. **H,** Schematic depicting the effects of single and double *BCOR*/*BCORL1* mutations on global PRC1.1 levels. Loss of BCOR-PRC1.1 in single $BCOR^{KO}$ cells results in a relative increase of BCORL1–PRC1.1. However, BCORL1 protein expression and therefore BCORL1–PRC1.1 levels remain low, resulting in decreased levels of global PRC1.1.

measured the depletion of PCGF1 in the unbound fractions. In BCOR-co-IP, BCOR and PCGF1 were both depleted from the unbound fraction (Fig. 2D). In contrast, in BCORL1-co-IP, BCORL1 was effectively depleted from the unbound fraction, but the abundance of PCGF1 was not visibly changed (Fig. 2D). These data indicate that PCGF1 predominantly binds to BCOR and that BCORL1–PRC1.1 contributes negligibly to global PRC1.1 levels in WT cells. In contrast, BCORL1 and PCGF1 were similarly depleted from the unbound fraction in $BCOR^{KO}$ cells, confirming that BCORL1 interacted with PCGF1 in the absence of BCOR (Fig. 2D).

Although we observed a relative increase of BCORL1–PRC1.1 in single *BCOR*-mutant cells, binding of KDM2B with the enzymatic core was decreased, indicating a quantitative loss of fully assembled PRC1.1 (Fig. 2C). We validated this finding in MOLM14 AML cells by KDM2B-co-IP analysis and confirmed reduced KDM2B binding to the enzymatic core in *BCOR*-mutant MOLM14 AML cells (Supplementary Fig. S1E). In contrast to *BCOR*-mutant cells, global PRC1.1 levels were not impaired in *BCORL1*-mutant cells (Supplementary Fig. S1F). We hypothesized that the differential impact of BCOR versus BCORL1 loss on fully assembled PRC1.1 levels was due to differences in the abundance of paralog expression. Consistent with this hypothesis, BCOR was expressed more highly than BCORL1 in WT K562 cells and we observed no compensatory increase of BCORL1 expression levels or protein levels in *BCOR*-mutant cells (Fig. 2C and E). More broadly, BCOR was the predominantly expressed paralog in other $BCOR/BCORL1^{WT}$ AML cell lines, in primary AML samples, and throughout normal hematopoiesis (Fig. 2F and G). Similar to our findings in K562 cells, we observed no compensatory increase of BCORL1 expression levels in *BCOR*-mutant primary patient samples (Supplementary Fig. S1G). Together, our data indicate that PRC1.1 levels are directly linked to the composite level of BCOR and BCORL1 expression levels and that reduction of fully assembled PRC1.1 in single *BCOR*- or *BCORL1*-mutant cells is proportional to the baseline expression levels of the remaining paralog (Fig. 2H). Therefore, BCORL1, which is lowly expressed in hematopoiesis, is insufficient to rescue the quantitative loss of global PRC1.1 levels in *BCOR*-mutant cells.

BCOR and BCORL1 Are Required for PCGF1 Stability

The similar effect of $BCOR^{KO}$ and $BCOR^{PUFD\text{-}Tr}$ mutations on PRC1.1 assembly suggested that the BCOR-PUFD domain is required for complex integrity. Consistent with this observation, BCOR/BCORL1-PUFD have been reported to interact directly with PCGF1-RAWUL, where this interaction was required for PCGF1-RAWUL stability *in vitro* (17). To define the impact of BCOR-PUFD:PCGF1 interaction on the stability of full-length PCGF1 *in vivo*, we analyzed the effects of *BCOR* and *BCORL1* mutations on PCGF1 abundance. In $BCOR^{KO}/BCORL1^{KO}$ and $BCOR^{PUFD\text{-}Tr}/BCORL1^{KO}$ cells, we observed complete loss of PCGF1 protein, despite no difference in PCGF1 mRNA level (Fig. 3A). In contrast, concurrent *BCOR*/*BCORL1* inactivation had no effect on the abundance of other PRC1 or PRC2 subunits (Fig. 3A). In agreement, PCGF1 protein levels were decreased in primary AML samples with *BCOR* mutations (Supplementary Fig. S2A) and we confirmed that disruption of PCGF1–BCOR–PUFD interactions was associated with reduced PCGF1 levels in BCOR PUFD-truncated MOLM14 AML cell lines (Supplementary Fig. S2B). These data indicate a specific requirement for the BCOR-PUFD domain for PCGF1 stability.

To determine whether BCOR-PUFD was alone sufficient to restore BCOR–PCGF1 interactions *in vivo*, we expressed HA-tagged BCOR-PUFD in $BCOR^{KO}/BCORL1^{KO}$ cells (Supplementary Fig. S2C). HA-BCOR-PUFD formed a stable heterodimer with PCGF1 and enabled interaction with RNF2 (Fig. 3B), demonstrating that PUFD was necessary and sufficient to bind PCGF1. Expression of an HA-tagged BCOR C-terminal fragment that included PUFD plus Ankyrin repeat and linker domains (BCOR-CT) restored not only PCGF1 binding and interaction with the enzymatic core but also BCOR interactions with KDM2B (Fig. 3C). Consistent with this finding, complementation of $BCOR^{KO}/BCORL1^{KO}$ cells with full-length BCOR restored PCGF1 protein levels and KDM2B interactions with the enzymatic core subunits (Supplementary Fig. S2D). Thus, our results indicate that BCOR and BCORL1 are essential to link the enzymatic core to KDM2B by binding and stabilizing PCGF1 protein.

We next sought to determine whether the effect of *BCOR* mutations on PRC1.1 assembly was explained solely by PCGF1 destabilization. We therefore generated a series of $PCGF1^{KO}$ cell lines (Fig. 3D) and defined BCOR-interacting proteins in the presence (WT) or absence of PCGF1 ($PCGF1^{KO}$) using IP and mass spectrometry (MS; Fig. 3E). In WT cells, the main interaction partners of BCOR were PRC1.1-defining and accessory subunits and pan-PRC1 enzymatic core subunits (Fig. 3E; Supplementary Fig. S2E–S2G). We did not identify BCOR interactions with BCL6 (18) or MLLT3 (AF9) in BCOR-co-IP MS, which have been shown to interact with BCOR in B cells (19–21) and MLL–AF9 rearranged leukemia (14, 15), respectively. In $PCGF1^{KO}$ cells, we observed selective loss of BCOR binding to the enzymatic core, including RING1, RNF2, RYBP, and CBX8 and no *de novo* or compensatory interaction partners (Fig. 3E; Supplementary Fig. S2E–S2G), confirming that highly specific PCGF1–BCOR/BCORL1 interactions are required to couple the enzymatic core to PRC1.1.

BCOR–PRC1.1 and BCORL1–PRC1.1 Complexes Are Independently Recruited via KDM2B to a Shared Set of Target Loci

We found that BCOR–PRC1.1 and BCORL1–PRC1.1 assemble independently and without apparent difference in complex constituency. To determine whether these distinct PRC1.1 species localize to similar or different chromatin sites, we performed BCOR and BCORL1 chromatin immunoprecipitation sequencing (ChIP-seq) in WT cells. BCOR and BCORL1 bound predominantly to promoter regions (Fig. 4A; Supplementary Fig. S3A), and their binding distributions at transcription start sites (TSS) were significantly correlated (Fig. 4B). BCORL1 binding was unchanged in $BCOR^{KO}$ cells compared with WT cells (Fig. 4A and B), and BCOR- and BCORL1-bound genes were co-occupied by the PRC1.1 subunits KDM2B and RNF2 (Fig. 4A), indicating that BCOR–PRC1.1 and BCORL1–PRC1.1 complexes are independently recruited to a shared set of target loci.

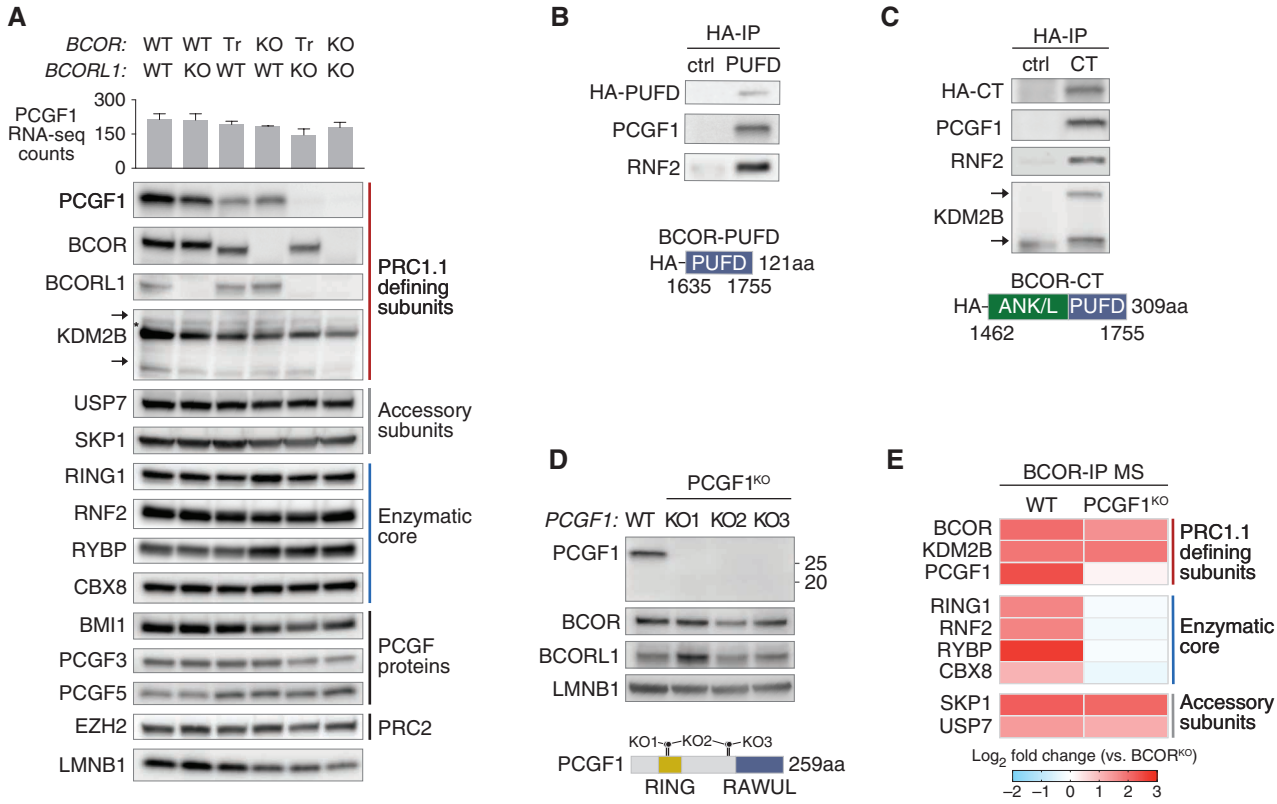

Figure 3. BCOR and BCORL1 are required for PCGF1 stability. **A,** PCGF1 gene expression (DESeq2-normalized counts) in the indicated cell lines (mean ± SD; top). Bottom, corresponding Western blot analysis of nuclear extracts. RNA-seq, RNA sequencing; Tr, PUFD-truncated. **B,** Co-IP–Western blot of exogenously expressed BCOR HA-PUFD (1635–1755 aa) in BCOR^{KO}/BCORL1^{KO} cells. Negative control was BCOR^{KO}/BCORL1^{KO} cells transduced with a control vector. **C,** Co-IP-Western blot of exogenously expressed BCOR HA-CT (1462–1755 aa) in BCOR^{KO}/BCORL1^{KO} cells. Negative control was BCOR^{KO}/BCORL1^{KO} cells transduced with a control vector. **D,** Western blot analysis of nuclear extracts from WT or PCGF1^{KO} K562 cells. *PCGF1* mutations are illustrated in the schematic (bottom). KO1, p.I60fs*; KO2, p.I60fs*/p.Y163fs*; KO3, p.Y163del. **E,** Enrichment of PRC1.1 subunits in BCOR-IP MS of WT or PCGF1^{KO} cells represented as $\log_2$ fold change compared with BCOR^{KO} control. $n = 2$ (process replicates for each condition). See also Supplementary Fig. S2E–S2G.

In human embryonic stem cells (ESC), PRC1.1 binding to most target genes has been reported to be dependent on RING1/RNF2 (22), while in mouse ESCs PRC1.1 recruitment is largely mediated by KDM2B (23–25). To determine the requirements for the PRC1.1 chromatin recruitment in human leukemia cells, we performed BCOR-ChIP-seq in WT cells or isogenic cell lines deficient for BCOR, PCGF1, or KDM2B. In both BCOR$^{PUFD\text{-}Tr}$ and PCGF1^{KO} cells, where BCOR is selectively uncoupled from the enzymatic core while retaining binding to KDM2B, BCOR recruitment to chromatin was similar compared to WT (Fig. 4C; Supplementary Fig. S3B and S3C). We validated this finding in primary patient samples, confirming that truncated BCOR maintained binding to target genes (Supplementary Fig. S3D). In contrast, KDM2B loss resulted in global loss of BCOR binding to chromatin (Fig. 4C; Supplementary Fig. S3C and S3E). KDM2B has been reported to bind to DNA via its CXXC zinc-finger domain, which recognizes unmethylated CpG islands (CGI; refs. 23–25). Consistent with the KDM2B-dependent recruitment mechanism, we found that BCOR and BCORL1 binding was enriched at unmethylated CGI promoters in K562 cells (Fig. 4D and E; Supplementary Fig. S3F), as well as in primary AML patient samples and in KG1, OCI-AML3, and MV411 AML cell lines (Supplementary Fig. S3G and S3H). Together, these data indicate that KDM2B, but not PCGF1 or the enzymatic core, is absolutely required for PRC1.1 recruitment in leukemia (Fig. 4F).

The PRC1.1 Enzymatic Core Is Required for Target Gene Repression

We next surveyed the chromatin state of PRC1.1-bound and PRC1.1-unbound genes using H3K27ac, H3K4me3, H3K27me3, and H2AK119ub ChIP-seq and Assay for Transposase-Accessible Chromatin sequencing (ATAC-seq). Among 11,934 PRC1.1-bound genes, 21.8% had a repressed chromatin state with high H3K27me3, high H2AK119ub, and low or no gene expression, and 78.2% had an active chromatin state (Fig. 5A and B; Supplementary Fig. S4A). We observed a similar distribution of BCOR binding in KG1, OCI-AML3, and MV411 cell lines and in primary AML patient cells (Supplementary Fig. S4B–S4D). However, PRC1 chromatin binding alone does not directly correlate with gene regulatory activity (23). To define the set of PRC1.1 functional targets, we therefore measured the effect of complete PRC1.1 inactivation on global gene expression. The predominant consequence of PRC1.1 loss was gene upregulation, irrespective of

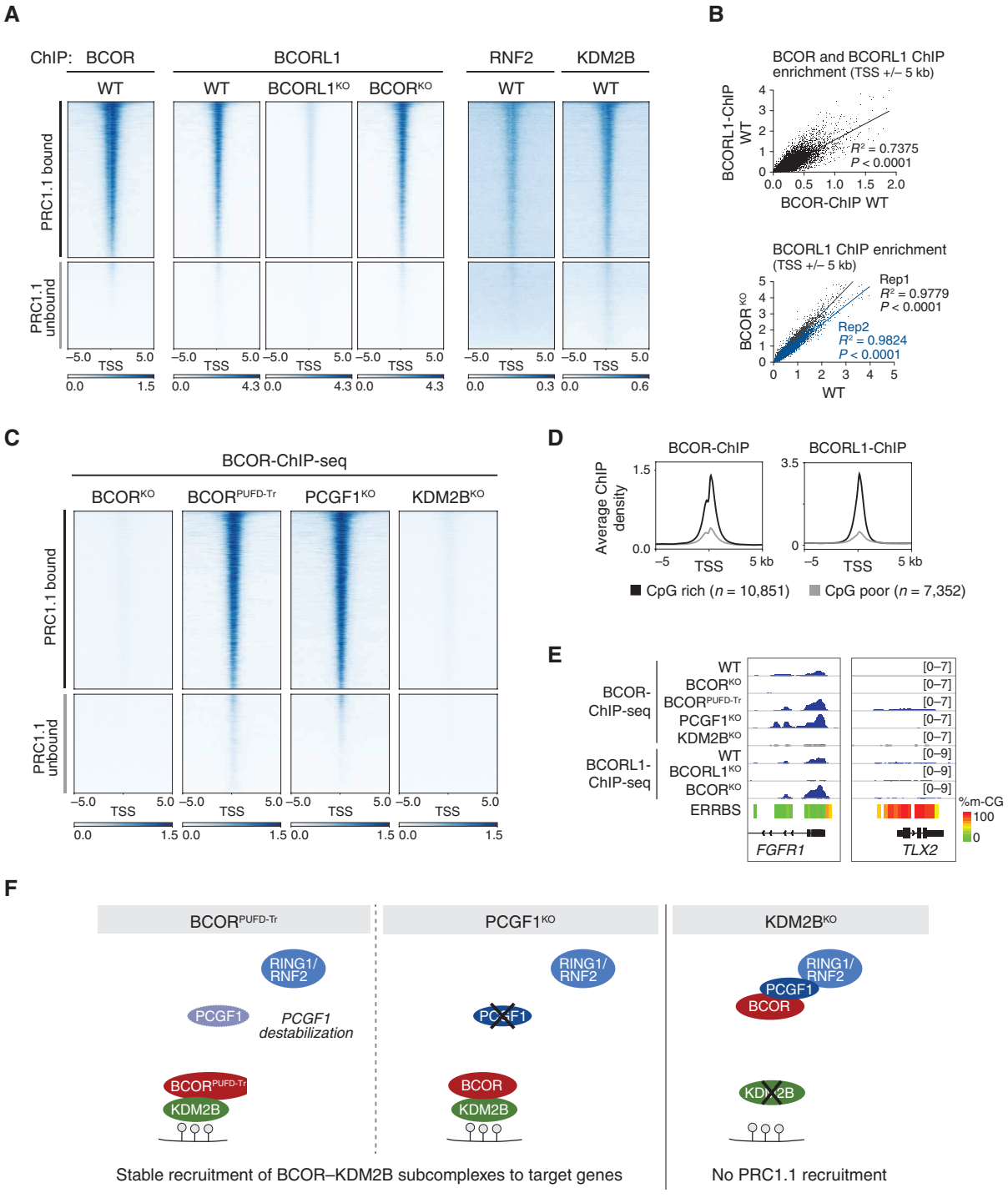

Figure 4. KDM2B is essential to recruit BCOR–PRC1.1 and BCORL1–PRC1.1 to unmethylated CpG island promoters. **A,** Heat maps represent ChIP enrichment at TSS ± 5 kb in WT, BCORL1^{KO}, or BCOR^{KO} K562 cells. BCOR-ChIP signal scores in WT cells were used to predefine PRC1.1 bound (n = 11,934) and PRC1.1 unbound (n = 6,639) promoters. All heat maps are sorted and ranked on the basis of BCOR-ChIP enrichment in WT cells. **B,** Scatter plots showing the relationship between BCORL1- and BCOR-ChIP-seq signals at TSS ± 5 kb in WT cells (top), and between BCORL1-ChIP-seq signals in BCOR^{KO} and WT cells (bottom). Biological replicates are plotted in black (Rep1) or in blue (Rep2). Pearson correlation coefficients and P values (two-tailed) as indicated. **C,** Heat maps of BCOR-ChIP-seq enrichment at PRC1.1 bound (n = 11,934) and PRC1.1 unbound (n = 6,639) gene promoters in BCOR^{KO}, BCOR$^{PUFD-Tr}$, PCGF1^{KO}, or KDM2B^{KO} cells. All heat maps are sorted and ranked on the basis of BCOR-ChIP signals in WT cells (**A**). **D,** Average density profiles of BCOR-ChIP and BCORL1-ChIP signals in WT cells at CpG-rich promoters (n = 10,851) or CpG-poor promoters (n = 7,352). **E,** Genomic coverage data tracks for BCOR-ChIP-seq and BCORL1-ChIP-seq at unmethylated (*FGFR1*) or methylated (*TLX2*) CGI promoters. Methylation percentages of CpG sites are indicated by the color gradient. **F,** Schematic of PRC1.1 recruitment in BCOR$^{PUFD-Tr}$, PCGF1^{KO}, and KDM2B^{KO} conditions. BCOR is stably recruited to target genes in BCOR$^{PUFD-Tr}$ and PCGF1^{KO} conditions but not in KDM2B^{KO} cells, indicating that KDM2B but not the enzymatic core is required for PRC1.1 recruitment in leukemia cells.

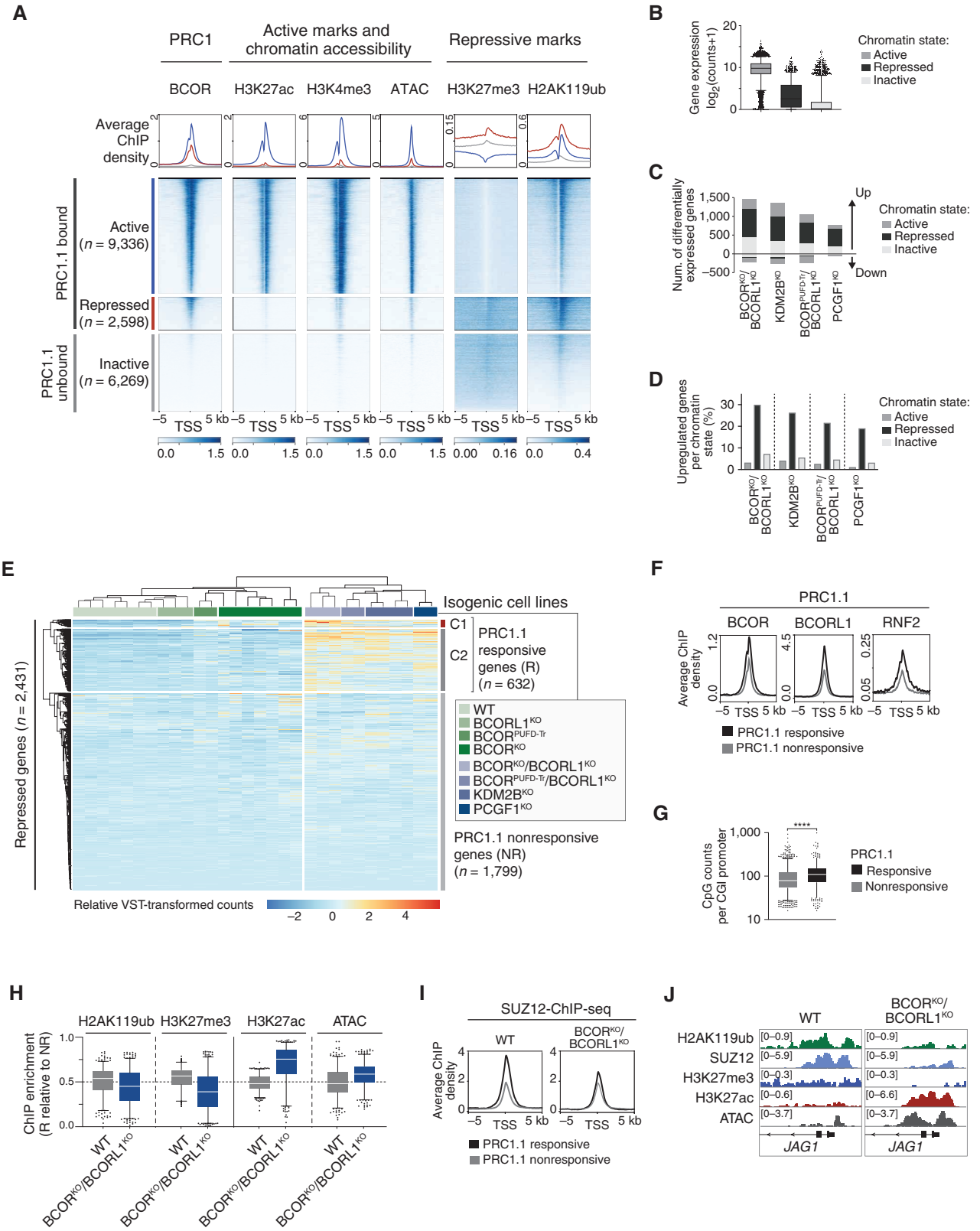
A
PRC1
Active marks and chromatin accessibility
Repressive marks
BCOR
H3K27ac
H3K4me3
ATAC
H3K27me3
H2AK119ub
Average ChIP density
PRC1.1 bound
Active (n = 9,336)
Repressed (n = 2,598)
PRC1.1 unbound
Inactive (n = 6,269)
–5 TSS 5 kb
B
Gene expression log2(counts+1)
Chromatin state:
Active
Repressed
Inactive
C
Num. of differentially expressed genes
Up
Down
BCOR KO/ BCORL1 KO
KDM2B KO
BCOR PUFD-Tr/ BCORL1 KO
PCGF1 KO
D
Upregulated genes per chromatin state (%)
E
Isogenic cell lines
Repressed genes (n = 2,431)
C1
C2
PRC1.1 responsive genes (R) (n = 632)
WT
BCORL1 KO
BCOR PUFD-Tr
BCOR KO
BCOR KO/BCORL1 KO
BCOR PUFD-Tr/BCORL1 KO
KDM2B KO
PCGF1 KO
PRC1.1 nonresponsive genes (NR) (n = 1,799)
Relative VST-transformed counts
F
PRC1.1
BCOR
BCORL1
RNF2
Average ChIP density
PRC1.1 responsive
PRC1.1 nonresponsive
G
CpG counts per CGI promoter
****
PRC1.1
Responsive
Nonresponsive
H
H2AK119ub
H3K27me3
H3K27ac
ATAC
ChIP enrichment (R relative to NR)
WT
BCOR KO/BCORL1 KO
I
SUZ12-ChIP-seq
Average ChIP density
J
WT
BCOR KO/ BCORL1 KO
H2AK119ub
SUZ12
H3K27me3
H3K27ac
ATAC
JAG1

the mechanism of complex inactivation, including complete PRC1.1 loss ($BCOR^{KO}$/$BCORL1^{KO}$), disruption of PRC1.1 recruitment to chromatin ($KDM2B^{KO}$), and selective uncoupling of the PRC1 enzymatic core ($BCOR^{PUFD\text{-}Tr}$/$BCORL1^{KO}$ and $PCGF1^{KO}$; Fig. 5C; Supplementary Fig. S4E). The relative impact of PRC1.1 inactivation was strongest among genes with a repressed chromatin state at baseline (Fig. 5C and D; Supplementary Fig. S4F), together indicating that PRC1.1 disruption causes selective derepression of target genes.

To identify a common set of PRC1.1 target genes in leukemia cells, we performed unsupervised hierarchical clustering in WT and all PRC1.1-mutant cells. Among genes with repressed chromatin at baseline, we identified two main clusters: PRC1.1-responsive genes ($n = 632$) and PRC1.1-nonresponsive genes ($n = 1{,}799$; Fig. 5E; Supplementary Fig. S4G). PRC1.1-responsive genes showed higher levels of H2AK119ub and H3K27me3, stronger binding of BCOR, BCORL1, and RNF2, and higher CpG levels at CGI promoters than PRC1.1-nonresponsive genes (Fig. 5F and G; Supplementary Fig. S4H), indicating that PRC1.1 is required to maintain repression of a defined set of CpG-rich target genes.

H2AK119ub deposition by noncanonical PRC1 has been reported to be essential to recruit PRC2 and to maintain repression of target genes (26–28). We hypothesized that PRC1.1 loss disrupted H2AK119ub deposition, resulting in epigenetic activation of PRC1.1-responsive leukemia target genes. Consistent with this hypothesis, we observed decreased H2AK119ub and H3K27me3 levels at PRC1.1-responsive genes in $BCOR^{KO}$/$BCORL1^{KO}$ cells compared with WT, while H3K27ac levels and chromatin accessibility were increased (Fig. 5H). PRC1.1 disruption and decreased H2AK119ub deposition at PRC1.1-responsive genes were further associated with reduced PRC2 occupancy (Fig. 5I and J), whereas global levels of H2AK119ub or PRC2 were not impaired (Supplementary Fig. S4I). These data suggest that PRC1.1 enzymatic activity maintains active repression of specific target genes by H2AK119ub deposition and stable recruitment of PRC2.

PRC1.1 Regulates Cell Signaling Programs in Human Leukemia

To identify PRC1.1-dependent transcription programs in human leukemia, we performed gene set enrichment analysis (GSEA) of differentially expressed genes in $BCOR^{KO}$/$BCORL1^{KO}$ compared with $BCOR^{WT}$/$BCORL1^{WT}$ cells. Differentially expressed genes in $BCOR^{KO}$/$BCORL1^{KO}$ conditions were enriched for signaling pathways regulating stem cell pluripotency [Kyoto Encyclopedia of Genes and Genomes (KEGG) KEGG hsa04550] including FGF/FGFR signaling, PI3K–Akt signaling, and TGFβ signaling pathways (Fig. 6A and B; Supplementary Fig. S5A and S5B), consistent with a role for PRC1.1 in regulating stem cell signaling programs. We further observed enrichment of signaling pathways involved in cancer (KEGG hsa05200) such as RAS and MAPK signaling pathways (Fig. 6A; Supplementary Fig. S5A and S5B). We validated our results in primary patient samples with ($n = 22$) and without ($n = 216$) *BCOR* mutations from the Beat AML study (29), confirming enrichment for regulators of stem cell pluripotency and cancer signaling pathways and higher gene expression levels of FGFR1, PDGFA, and FOXO1 in samples with *BCOR* mutations (Fig. 6C and D; Supplementary Fig. S5C and S5D). Using Western blot analysis, we confirmed high FGFR1 protein levels in *BCOR*-mutant AML patient cells (Supplementary Fig. S5E). Consistent with these results, we found that the PRC1.1 target genes *JAG1* and *FOXO1* had a repressed chromatin state (high H3K27me3 and H2AK119ub) and were lowly expressed in primary $BCOR^{WT}$ AML blasts, whereas these genes were associated with an active chromatin state in primary $BCOR^{PUFD\text{-}Tr}$ AML blasts (Fig. 6E; Supplementary Fig. S5F). Together, these data indicate that PRC1.1 inactivation in *BCOR*-mutated AML results in aberrant expression of stem cell signaling programs via epigenetic derepression of target genes.

Sole *BCOR* Mutation Activates Highly Responsive PRC1.1 Target Genes

BCOR mutations are commonly found without concurrent *BCORL1* mutations in patients with myeloid malignancies, suggesting that partial PRC1.1 disruption is sufficient to drive disease progression. To define target genes that were responsive to quantitative decreases in PRC1.1 abundance, we compared the effect of single *BCOR* mutations versus double *BCOR*/*BCORL1* mutations on gene expression and found that a subset of genes that were upregulated in double *BCOR*/*BCORL1*-mutant conditions were also induced in

Figure 5. Recruitment of the PRC1.1 enzymatic core is required for target gene repression. **A,** Heat maps and profile plots of ChIP-seq enrichment of BCOR, histone modifications, and chromatin accessibility signals (ATAC) as indicated. BCOR-ChIP signal scores in K562 WT cells were used to predefine PRC1.1-bound promoters ($n = 11{,}934$). BCOR- and H3K27ac-ChIP signal scores in WT cells were used to define active, repressed, and inactive gene promoters. K562 H3K4me3-ChIP-seq data were downloaded from the Sequence Read Archive (SRA; SRR341173). The remaining datasets were generated in this study. **B,** Gene expression levels (DESeq2-normalized counts) of active, repressed, or inactive genes in K562 cells. BCOR- and H3K27ac-ChIP signal scores in K562 WT cells were used to define active, repressed, and inactive chromatin states (as depicted in **A**). The line in the middle of the box represents the median, box edges represent the 25th and 75th percentiles, and whiskers show 5th and 95th percentiles. **C,** Number (num.) of differentially expressed genes in PRC1.1-mutant compared with WT cells (fold change > 2, $P_{adj} < 0.05$). Differentially expressed genes were subdivided on the basis of their chromatin states defined in **A**. **D,** Bar diagram represents the percentages of upregulated genes in PRC1.1-mutant cells relative to the total number of genes in each chromatin state. **E,** Unsupervised hierarchical clustering of expression levels of PRC1.1-bound repressed genes in WT ($n = 7$) or PRC1.1-mutant cells [$BCORL1^{KO}$ ($n = 3$), $BCOR^{PUFD\text{-}Tr}$ ($n = 2$), $BCOR^{KO}$ ($n = 7$), $BCOR^{KO}$/$BCORL1^{KO}$ ($n = 3$), $BCOR^{PUFD\text{-}Tr}$/$BCORL1^{KO}$ ($n = 2$), $KDM2B^{KO}$ ($n = 4$), and $PCGF1^{KO}$ ($n = 2$)]. Genes clustered into PRC1.1-responsive ($n = 632$) or PRC1.1-nonresponsive ($n = 1{,}799$) genes. PRC1.1-responsive genes clustered into cluster 1 (C1; $n = 65$) or cluster 2 (C2; $n = 567$) genes. Gene expression levels are shown as relative variance stabilizing transformation (VST)–transformed values. **F,** Average density profiles of BCOR-, BCORL1- and RNF2-ChIP signals in WT cells at PRC1.1-responsive ($n = 632$) or PRC1.1-nonresponsive genes ($n = 1{,}799$). **G,** Number of CpG counts at PRC1.1-responsive ($n = 632$) or PRC1.1-nonresponsive CGI promoters ($n = 1{,}799$). ****, $P < 0.0001$, unpaired *t* test. The line in the middle of the box represents the median, box edges represent the 25th and 75th percentiles, and whiskers show 5th and 95th percentiles. **H,** Box and whisker plots representing histone ChIP- and ATAC-seq signals at PRC1.1-responsive genes ($n = 632$) normalized to the signals at PRC1.1-nonresponsive genes ($n = 1{,}799$) in WT or $BCOR^{KO}$/$BCORL1^{KO}$ cells. The line in the middle of the box represents the median, box edges represent the 25th and 75th percentiles, and whiskers show 2.5th and 97.5th percentiles. **I,** Average density profiles of SUZ12-ChIP signals in WT or $BCOR^{KO}$/$BCORL1^{KO}$ cells at PRC1.1-responsive ($n = 632$) or PRC1.1-nonresponsive genes ($n = 1{,}799$). **J,** ChIP-seq and ATAC-seq coverage data tracks of the PRC1.1-responsive gene *JAG1* in WT or $BCOR^{KO}$/$BCORL1^{KO}$ cells.

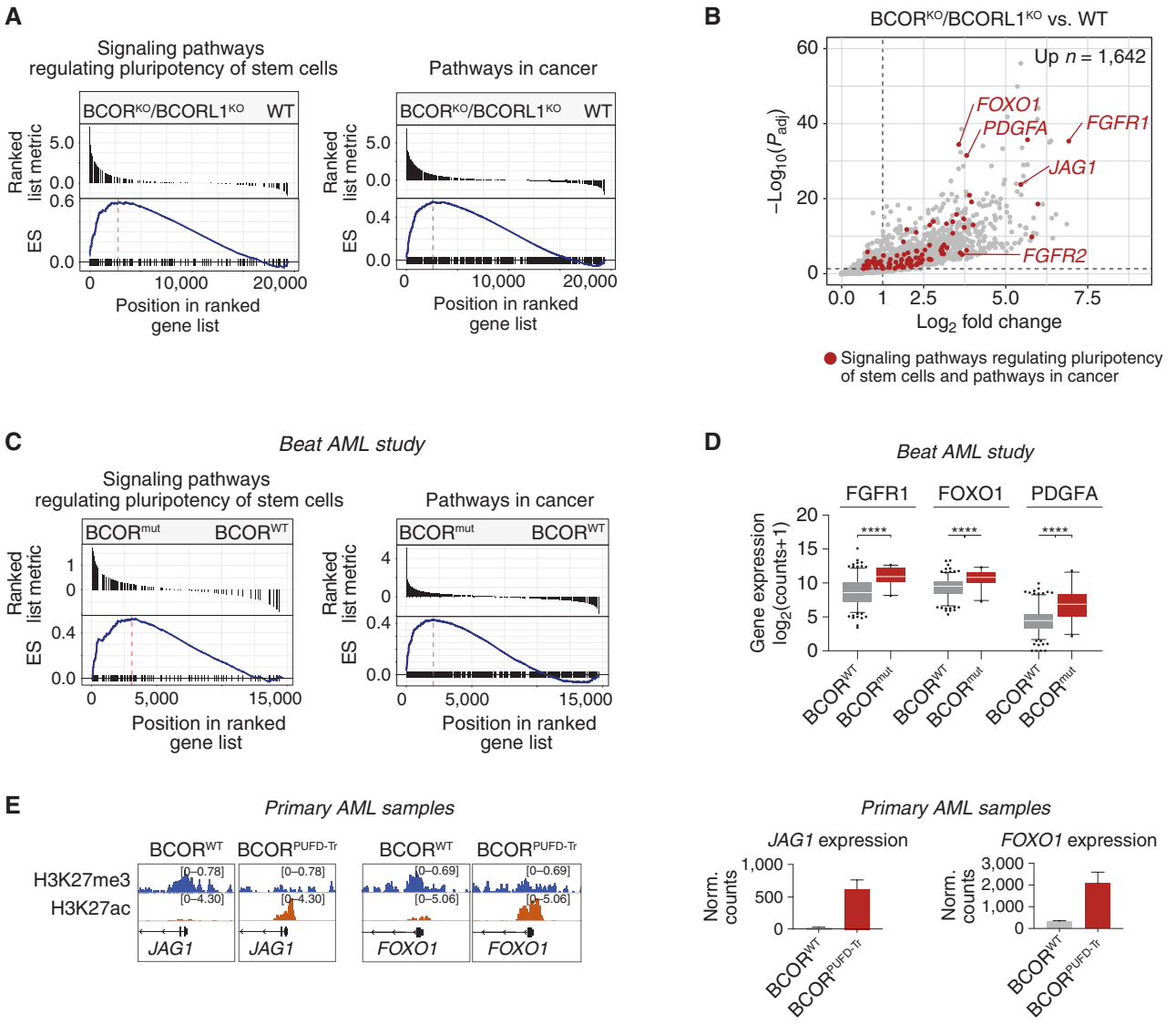

Figure 6. PRC1.1 regulates cell signaling programs in human leukemia. **A,** KEGG GSEA of differentially expressed genes in BCOR^{KO}/BCORL1^{KO} compared with WT K562 cells. The top plot represents the magnitude of $\log_2$ fold changes for each gene. The bottom plot indicates the enrichment score (ES). **B,** Volcano plot representing gene expression changes of upregulated genes in BCOR^{KO}/BCORL1^{KO} compared with WT cells. Genes represented in KEGG signaling pathways regulating pluripotency of stem cells (hsa04550) or KEGG pathways in cancer (hsa05200) are highlighted in red. $\log_2$ fold changes of 1 and P_{adj} values of 0.05 are depicted by dotted lines. A total of 1,642 genes were significantly upregulated more than twofold in BCOR^{KO}/BCORL1^{KO} cells compared with WT control. **C,** KEGG GSEA of differentially expressed genes in BCOR^{mut} ($n = 22$) compared with BCOR^{WT} ($n = 216$) AML patient samples from the Beat AML study (29). See also Supplementary Fig. S5C. **D,** Box and whisker plots representing expression levels [$\log_2$-transformed DESeq2-normalized (norm.) counts] in BCOR^{WT} ($n = 216$) or BCOR^{mut} ($n = 22$) primary AML samples (29). ****, $P < 0.0001$, Wilcoxon rank-sum test. The line in the middle of the box represents the median, box edges represent the 25th and 75th percentiles, and whiskers show 5th and 95th percentiles. **E,** ChIP-seq coverage data tracks of PRC1.1 target genes *JAG1* and *FOXO1* in BCOR^{WT} (Pt.1) or BCOR$^{PUFD\text{-}Tr}$ (Pt.5) cells (left). Corresponding gene expression levels of *JAG1* and *FOXO1* [DESeq2-normalized (norm.) counts, right; $n = 2$, technical replicates].

single BCOR mutants (Fig. 7A; Supplementary Fig. S6A). On the basis of their sensitivity to partial PRC1.1 inactivation, responsive genes could be classified into two groups: cluster 1 (C1; $n = 65$) genes showed significantly higher expression in single BCOR^{KO} and double BCOR^{KO}/BCORL1^{KO} cells compared with cluster 2 (C2; $n = 567$) genes and were significantly more highly expressed in double BCOR^{KO}/BCORL1^{KO} cells than in single BCOR^{KO} cells (Fig. 5E and Fig. 7B). PRC1.1 reduction in single *BCOR*-mutant cells is thus sufficient to activate a subset of highly responsive PRC1.1 target genes, whereas complete PRC1.1 loss in BCOR^{KO}/BCORL1^{KO} cells results in activation of the full set of target genes.

Within the C1 gene cluster, *FGFR1* was among the most highly upregulated genes in partially as well as fully deficient PRC1.1-mutant cells (Fig. 7C; Supplementary Fig. S6B). At baseline, the *FGFR1* locus had a repressed chromatin state marked by low accessibility, enrichment of H2AK119ub and H3K27me3, and absent H3K27ac (Fig. 7D). Accordingly,

there was no *FGFR1* transcription and no detectable FGFR1 protein (Fig. 7E). Partial PRC1.1 inactivation in BCOR^{KO} and BCOR$^{PUFD\text{-}Tr}$ cells caused significantly increased FGFR1 expression without epigenetic reprogramming, whereas complete disruption of PRC1.1 in BCOR^{KO}/BCORL1^{KO}, BCOR$^{PUFD\text{-}Tr}$/BCORL1^{KO}, PCGF1^{KO}, and KDM2B^{KO} caused loss of repressive histone marks and increased chromatin accessibility that correlated with a significant increase in FGFR1 gene expression and protein levels (Fig. 7D and E). To confirm this observation in an independent AML cell line model, we generated MOLM13 cells with BCOR^{KO}, BCORL1^{KO}, BCOR^{KO}/BCORL1^{KO}, or KDM2B^{KO} and found that PRC1.1 inactivation caused similar activation of FGFR1 expression (Supplementary Fig. S6C). To determine whether the effect of PRC1.1 inactivation on FGFR1 expression was reversible and maintained dependency on intact BCOR/PRC1.1, we expressed a single-guide RNA (sgRNA)–resistant full-length BCOR cDNA in BCOR^{KO}/BCORL1^{KO} cells. Complementation of BCOR expression restored PRC1.1 complex assembly (Supplementary Fig. S2D) and decreased FGFR1 protein levels in PRC1.1-deficient cells (Supplementary Fig. S6D).

PRC1.1 Mutations Drive Aberrant FGFR1 Activation that Mediates Resistance to Targeted Therapy

Upregulation of FGFR1 expression has been reported to be a mechanism of resistance to tyrosine kinase inhibition (30–32), and *BCOR* mutations have been specifically linked to CML blast phase and resistance to BCR–ABL-targeted inhibitors (10). We therefore hypothesized that PRC1.1 disruption drives resistance to targeted BCR–ABL inhibition via derepression of FGFR1. To test this hypothesis, we assessed the relative growth of PRC1.1-deficient cells compared with control cells using *in vitro* competition assays. We mixed fluorochrome-labeled control cells (Cas9 plus nontargeting sgRNA) and competitor cells (Cas9 plus sgRNA targeting *BCOR*, *BCORL1*, *BCOR*/*BCORL1*, or *KDM2B*) at an 80:20 ratio, then used flow cytometry to measure their relative proportion over 10 days with or without the addition of inhibitors (Fig. 7F). In baseline conditions, PRC1.1-mutated cells did not have a selective growth advantage compared with control cells (Fig. 7G). In contrast, when we blocked BCR–ABL signaling with imatinib, BCOR^{KO}, BCOR^{KO}/BCORL1^{KO}, and KDM2B^{KO} cells all showed selective growth advantage, indicating increased relative tyrosine kinase inhibitor (TKI) resistance (Fig. 7G). Single BCOR^{KO} cells that showed less pronounced activation of signaling genes, including *FGFR1* (Fig. 7C and E), were less resistant to imatinib than BCOR^{KO}/BCORL1^{KO} or KDM2B^{KO} cells, reflected by the lower proportion of BFP-positive cells at day 10 (BCOR^{KO}: 27.5%; BCOR^{KO}/BCORL1^{KO}: 52.1%; KDM2B^{KO}: 49.7%; Fig. 7G). In each competitor condition, we observed a concomitant increase in indel fraction at the sgRNA target sites (Supplementary Fig. S6E).

To determine whether the effect of PRC1.1 inactivation on imatinib resistance was mediated directly by FGFR1, we measured functional consequences of augmenting or inhibiting FGFR1 signaling. Supplementation of media with FGF2 (10 ng/mL) augmented the magnitude of selective advantage of BCOR^{KO}, BCOR^{KO}/BCORL1^{KO}, and KDM2B^{KO} cells compared with control cells (Fig. 7G) and was correlated with high FGFR1 protein levels at day 13 (Supplementary Fig. S6F). In contrast, concurrent treatment of cells with imatinib and the selective small-molecule FGFR1 inhibitor PD173074 completely abrogated resistance of BCOR^{KO}/BCORL1^{KO} cells compared with cells treated with imatinib alone (Fig. 7H). Treatment of K562 cells with PD173074 alone had no effect on cell growth or survival (Supplementary Fig. S6G). Together, these data indicate that genetic inactivation of PRC1.1 drives imatinib resistance via its effects on FGFR1.

To test whether selective uncoupling of the enzymatic core from target genes was sufficient to drive imatinib resistance, we performed *in vitro* competition assay using competitor sgRNAs targeting *BCOR exon 14* (BCOR^{PUFD}) which resulted in expression of PUFD-truncated BCOR (BCOR$^{PUFD\text{-}Tr}$; Supplementary Fig. S6H). When treated with imatinib, we observed a selective competitive advantage of single BCOR$^{PUFD\text{-}Tr}$ and double BCOR$^{PUFD\text{-}Tr}$/BCORL1^{KO} cells compared with WT control that was similar to BCOR^{KO} and BCOR^{KO}/BCORL1^{KO}conditions (Fig. 7I; Supplementary Fig. S6I), and which was completely inhibited by simultaneous treatment with imatinib and the FGFR inhibitor PD173074 (Supplementary Fig. S6J). These data confirm that PUFD-truncating *BCOR* mutations that selectively uncouple the enzymatic core from PRC1.1 target genes drive imatinib resistance via derepression of FGFR1, which is functionally equivalent to complete BCOR loss.

DISCUSSION

Here, we paired genetic analysis of 6,162 primary patient samples with functional studies in cell lines and primary AML samples to define the role of PRC1.1 alterations in leukemia pathogenesis. We found that BCOR and BCORL1 are central adapters that are required for PRC1.1 complex assembly and target gene repression. Leukemia-associated *BCOR* and *BCORL1* mutations cooperate to drive disease progression by selectively unlinking the enzymatic RING/PCGF1 core from the complex, thereby causing a quantitative reduction of enzymatically active PRC1.1 at chromatin and driving aberrant activation of oncogenic signaling programs. We demonstrate further that derepression of PRC1.1 target genes in *BCOR*/*BCORL1*-mutated CML cells mediates a functional resistance to kinase inhibitor treatment that is reversible with FGFR1 inhibition.

We show that pathogenic *BCOR* mutations share a unifying molecular mechanism for their epigenetic and oncogenic effects despite having diverse consequences on BCOR protein expression. Specifically, leukemia-associated *BCOR* mutations cause loss of a stabilizing interaction between the C-terminal BCOR-PUFD domain and the PRC1.1-specific adaptor PCGF1, which results in separation of the enzymatic core of PRC1 from the chromatin-targeted PRC1.1 auxiliary subcomplex. This paradigm is exemplified by *BCOR* mutations in patients that result in highly expressed PUFD-truncated BCOR proteins that are functional knockouts that lose tumor suppressor function. We show in both patient samples and engineered cell line models that these PUFD-truncating *BCOR* mutations disrupt PCGF1 binding and stability and result in derepression of a core set of PRC1.1 targets.

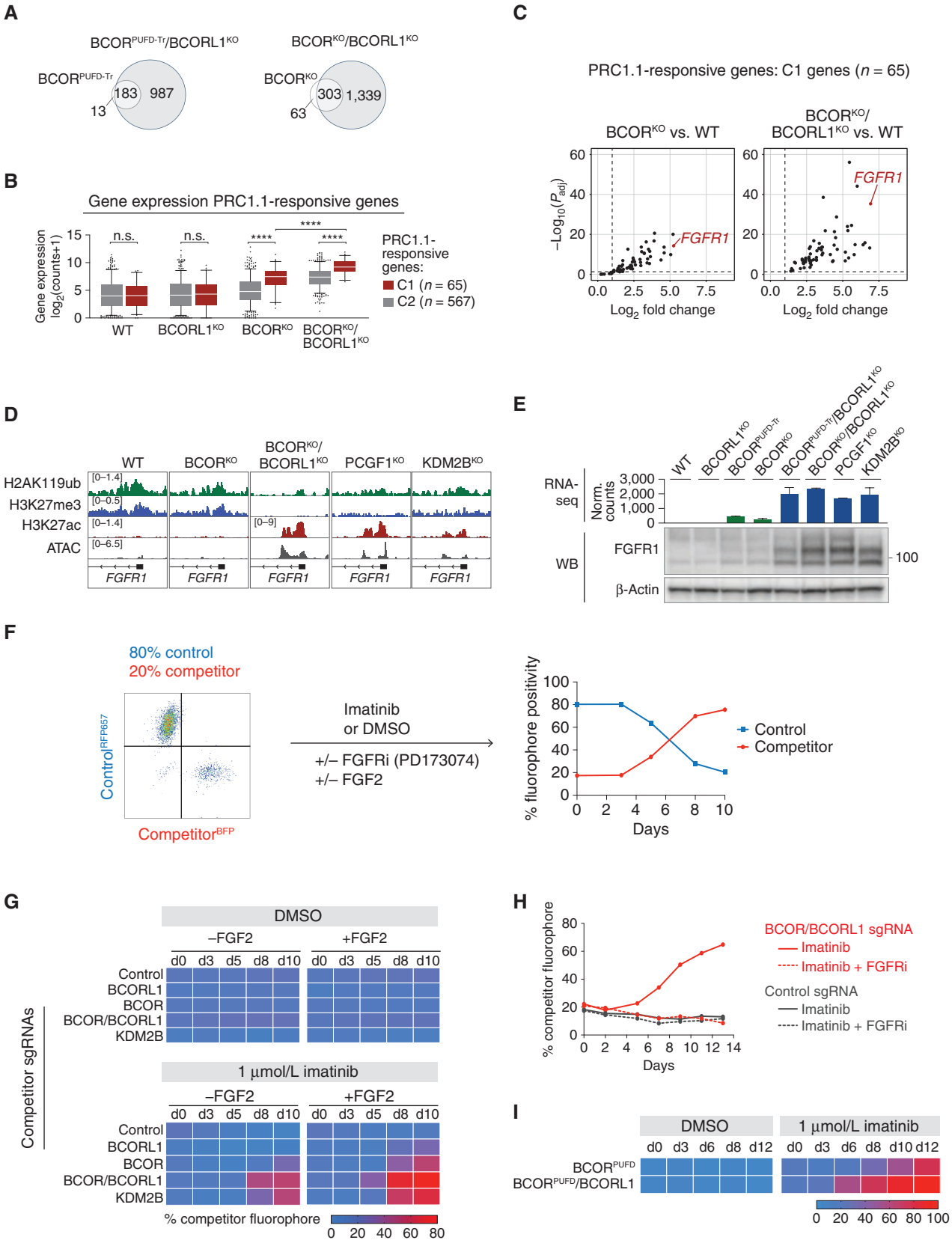
A
BCOR^PUFD-Tr/BCORL1^KO
BCOR^PUFD-Tr
183
987
13
BCOR^KO/BCORL1^KO
BCOR^KO
303
1,339
63
B
Gene expression PRC1.1-responsive genes
Gene expression log2(counts+1)
n.s.
n.s.
****
****
****
PRC1.1-responsive genes:
C1 (n = 65)
C2 (n = 567)
WT
BCORL1^KO
BCOR^KO
BCOR^KO/BCORL1^KO
C
PRC1.1-responsive genes: C1 genes (n = 65)
BCOR^KO vs. WT
BCOR^KO/BCORL1^KO vs. WT
−Log10(Padj)
FGFR1
Log2 fold change
D
WT
BCOR^KO
BCOR^KO/BCORL1^KO
PCGF1^KO
KDM2B^KO
H2AK119ub
H3K27me3
H3K27ac
ATAC
FGFR1
E
RNA-seq
Norm. counts
WB
FGFR1
β-Actin
100
F
80% control
20% competitor
Control^RFP657
Competitor^BFP
Imatinib or DMSO
+/− FGFRi (PD173074)
+/− FGF2
% fluorophore positivity
Days
Control
Competitor
G
DMSO
–FGF2
+FGF2
d0 d3 d5 d8 d10
Control
BCORL1
BCOR
BCOR/BCORL1
KDM2B
Competitor sgRNAs
1 µmol/L imatinib
% competitor fluorophore
H
% competitor fluorophore
Days
BCOR/BCORL1 sgRNA
Imatinib
Imatinib + FGFRi
Control sgRNA
Imatinib
Imatinib + FGFRi
I
DMSO
1 µmol/L imatinib
d0 d3 d6 d8 d12
d0 d3 d6 d8 d10 d12
BCOR^PUFD
BCOR^PUFD/BCORL1

Our results indicate that aggregate PRC1.1 tumor-suppressive activity in normal cells reflects a composite of BCOR–PRC1.1 and BCORL1–PRC1.1 repressive function. These distinct and mutually exclusive PRC1.1 species are composed of the same constituent proteins, localize to the same set of chromatin targets, and are functionally redundant. In leukemia, *BCOR* and *BCORL1* mutations cooperate by progressive reduction of PRC1.1 levels and a dose-dependent derepression of PRC1.1 target genes. We show that since BCOR is more highly expressed than BCORL1 in hematopoiesis, *BCOR* mutations cause a more pronounced quantitative reduction of global PRC1.1 levels than *BCORL1* mutations that drives transcriptional activation of a set of highly responsive PRC1.1 target genes. This finding provides a mechanistic explanation for the higher frequency of *BCOR* mutations in leukemia and for the observations that *BCORL1* mutations most commonly arose subclonally to a preexisting *BCOR* mutation in clonal evolution and mediate clinical progression.

We demonstrate that uncoupling of the PRC1.1 enzymatic core from target genes results in loss of H2AK119ub and PRC2 binding that drives transcriptional activation. Our data is in line with previous studies in mouse ESCs showing that H2AK119ub deposition by noncanonical PRC1 complexes was critical for target gene repression and PRC2 recruitment (26–28). In addition, we observed PRC1.1 binding to active gene promoters. These data are consistent with a study from Boom and colleagues demonstrating that PRC1.1 was enriched at active gene promoters in AML, suggesting a role in regulating active gene expression (33). However, we did not detect changes in expression levels of active genes upon PRC1.1 disruption in our cell line model. We therefore favor a model proposed by Farcas and colleagues in which PRC1.1 may sample CpG-rich gene promoters for susceptibility to polycomb-mediated silencing independent of their chromatin states, whereas additional factors are required to facilitate gene repression (23).

We used cell line models and primary AML samples to show that *BCOR*/*BCORL1* mutations, and PRC1.1 deficiency more broadly, were associated with activation of cell signaling pathways regulating stem cell pluripotency. This finding is consistent with the proposed role of PRC1.1 in normal regulation of stem cell transcriptional programs (22, 34) and raised the possibility that PRC1.1 mutations may confer sensitivity to targeted inhibition of RAS/MAPK signaling. Consistent with this model, epigenetic activation of the PRC1.1 target gene *FGFR1* mediated imatinib resistance in PRC1.1-deficient BCR–ABL-positive K562 cell lines that could be overcome by FGFR1 inhibition, explaining previous reports demonstrating that activation of FGFR signaling was a mechanism of TKI resistance in K562 cells (30) and that *BCOR* and *BCORL1* mutations were associated with blast crisis in patients with CML (10). PRC1.1-deficient cells thus maintain cell signaling and survival in the absence of BCR–ABL signaling by utilizing FGFR1 as an alternative signaling pathway. Our data provide a mechanistic framework in which disruption of PRC1.1 translates into an oncogenic phenotype by epigenetic activation of signaling target genes. Further studies are needed to systematically define therapeutic vulnerabilities in PRC1.1-deficient myeloid malignancies, including *BCOR*/*BCORL1*-mutated AML.

In conclusion, we show that somatic *BCOR* and *BCORL1* mutations disrupt PRC1.1 complex assembly, thereby inactivating normal PRC1.1 tumor suppression through derepression of a stem cell signaling transcription program. *BCOR* and *BCORL1* mutations define a group of PRC1.1-deficient myeloid malignancies that may respond to pharmacologic inhibition of hyperactive RAS/MAPK signaling, thereby limiting disease progression or mitigating secondary resistance to targeted therapies.

METHODS

Patient Samples

All patients provided written informed consent in accordance with the Declaration of Helsinki, and studies were approved by the Institutional Review Board at the Dana-Farber Cancer Institute (Boston, MA). Leukemic blasts were isolated from whole blood using CD3 depletion (StemCell Technologies) and ficoll density gradient separation.

Cell Lines

K562 cells (female) were acquired from the Broad Institute, and MV411 (male) and MOLM14 cells (male) were from James Griffin's lab. KG-1 (male) and OCI-AML3 cells (male) were purchased from ATCC. MOLM13 cells (male) were purchased from DSMZ. Cells were cultured in RPMI 1640 medium (Gibco) with 10% FBS (Sigma-Aldrich) and 1% penicillin–streptomycin–glutamine (PSG; Gibco) at 37°C and 5% CO_2. Cell lines were used within 4 to 8 weeks after thawing in the described experiments. All cell lines were authenticated

Figure 7. PRC1.1 mutations drive aberrant FGFR1 activation that mediates resistance to targeted therapy. **A,** Venn diagrams represent the overlaps of significantly upregulated genes in PRC1.1-mutant cells versus WT control. **B,** Box and whisker plots representing expression levels (log_2-transformed DESeq2-normalized counts) of C1 ($n = 65$) and C2 ($n = 567$) genes in WT, BCORL1^{KO}, BCOR^{KO}, or BCOR/BCORL1^{KO} cells. C1 and C2 genes were defined using unsupervised hierarchical clustering of expression levels of PRC1.1-responsive genes in WT or PRC1.1-mutant cells shown in Fig. 5E. The line in the middle of the box represents the median, box edges represent the 25th and 75th percentiles, and whiskers show 5th and 95th percentiles. Wilcoxon rank-sum test was used for statistical analysis. n.s., $P > 0.05$; ****, $P < 0.0001$. **C,** Volcano plots representing gene expression changes of upregulated genes in BCOR^{KO} versus WT (left) and BCOR^{KO}/BCORL1^{KO} versus WT (right) K562 cells. Only PRC1.1-responsive genes of cluster C1 ($n = 65$) are shown. Log_2 fold changes of 1 and P_{adj} values of 0.05 are depicted by dotted lines. **D,** ChIP-seq and ATAC-seq coverage data tracks of the PRC1.1-responsive gene *FGFR1* in WT or PRC1.1-mutant cells. **E,** *FGFR1* gene expression levels [normalized (norm.) DESeq2 counts] in WT or PRC1.1-mutant cells (top) represented as mean ± SEM. Corresponding Western blot (WB) analysis of FGFR1 protein levels (bottom; FGFR1: 91 kDa, glycosylated FGFR1: 120 kDa). RNA-seq, RNA sequencing. **F,** Schematic of the experimental workflow for *in vitro* competition assays. We mixed fluorochrome-labeled control cells (Cas9 plus nontargeting sgRNA) and competitor cells (Cas9 plus sgRNA targeting *BCOR*, *BCORL1*, *BCOR/BCORL1*, or *KDM2B*) at an 80:20 ratio, and then used flow cytometry to measure their relative proportion over 10 to 12 days with or without the addition of inhibitors and FGF2. **G,** Heat maps representing competitor percentages over the course of 10 days. Cells were cultured in the presence of DMSO (top) or 1 μmol/L imatinib (bottom) with or without FGF2 supplementation (10 ng/mL). **H,** Percentages of competitor cells expressing sgRNAs targeting *BCOR/BCORL1* (highlighted in red) or nontargeting control (highlighted in dark gray) over time. Cells were treated with 1 μmol/L imatinib alone (solid line) or with 1 μmol/L imatinib and 1 μmol/L FGFR inhibitor (FGFRi; PD173074) in combination (dotted line). **I,** Heat maps representing percentages of competitor cells expressing sgRNAs targeting BCOR^{PUFD} over the course of 12 days. Cells were cultured in the presence of DMSO (left) or 1 μmol/L imatinib (right) with FGF2 supplementation (10 ng/mL).

before use. *Mycoplasma* contamination was excluded using the MycoAlert *Mycoplasma* Detection Kit (Lonza).

DNA Sequencing

We prepared DNA from bone marrow aspirate samples obtained from 433 patients with newly diagnosed AML prior to treatment. We performed targeted sequencing of 113 genes known to be recurrently mutated in AML or in germline syndromes predisposing to development of myeloid malignancies. Native genomic DNA was sheared and the library constructed per manufacturer protocol (Agilent). Libraries were then quantified and pooled up to 24 samples per lane in equimolar amounts totaling 500 ng of DNA. Each pool was then hybridized to Agilent Custom SureSelect In Solution Hybrid Capture RNA baits. Each capture reaction was washed, amplified, and sequenced on an Illumina HiSeq 2000 100-bp paired-end run.

Fastq files were aligned to hg19 version of the human genome with Burrows-Wheeler Aligner (BWA) version 0.6.2 (35). Single nucleotide and small insertion and deletion calling was performed with samtools version 0.1.18 mpileup (36) and Varscan version 2.2.3 (37). Pindel version 0.2.41.2 (38) was used for FLT3-ITD calling at the specific genomic locus located at chromosome 13:28,608,000–28,608,600. Variants were annotated to include information about cDNA and amino acid changes, sequence depth, number and percentage of reads supporting the variant allele, population allele frequency in the genome aggregation database (gnomAD), and presence in Catalogue of Somatic Mutations in Cancer version 64. Variants were excluded if they had fewer than 15 total reads at the position, had fewer than five alternate reads, had variant allele fraction <2%, fell outside of the target coordinates, had excessive read strand bias, had an excessive number of calls in the local region, caused synonymous changes, or were recurrent small insertions/deletions at low variant allele fraction adjacent to homopolymer repeat regions. No germline tissue was available for evaluation of somatic status of mutations.

Generation of PRC1.1-Mutant Cell Lines

PRC1.1-mutant cell lines were generated using CRISPR/Cas9 ribonucleoprotein transient transfection or stable lentiviral transduction of a sgRNA-expressing construct.

For CRISPR/Cas9 ribonucleoprotein transient transfection, CRISPR RNA (crRNA) targeting *BCOR*, *PCGF1*, or control was mixed in equimolar concentrations with transactivating CRISPR RNA (tracrRNA) and heated at 95°C for 5 minutes. Ribonucleoprotein (RNP) complexes were prepared by mixing complexed crRNA:tracrRNA oligos, Cas9–NLS protein, and Cas9 working buffer, followed by incubation at room temperature for 20 minutes. K562 cells were resuspended in Nucleofector SF solution and then mixed with RNP complexes. The nucleofection mix was transferred to a Nucleocuvette strip and run on a Nucelofector 4D device.

For lentiviral production and stable cell line transduction, lentiviral vectors containing sgRNA-targeting *BCOR*, *BCORL1*, *PCGF1*, *KDM2B*, or control and lentiviral packaging plasmids (psPAX2: Addgene #12260; pCMV-VSV-G: Addgene #8454) were cotransfected into HEK293T cells. Lentiviral vectors were concentrated by ultracentrifugation at 25,000 rpm for 2 hours and resuspended in plain DMEM (Gibco). For lentiviral infection, cells were plated with 4 μg/mL polybrene (MilliporeSigma) and prepared lentivirus and spinfected at 2,000 rpm, 37°C for 2 hours. After 48-hour incubation, cells were selected on the basis of antibiotic resistance using 2 μg/mL puromycin (MilliporeSigma) or fluorophore expression by FACS sorting using Aria II SORP (BD).

PRC1.1-mutant K562 single-cell clones were derived from parental K562 cells harboring an N-terminal in-frame V5-tag integrated by Cas9 RNP-mediated homologous directed repair at the endogenous BCOR locus as described previously (39). Single-cell clones were isolated by limiting dilution, expanded, and screened by Sanger sequencing and TIDE (Tracking of Indels by DEcomposition) analysis (40). Single-cell clones with homozygous or compound heterozygous mutations in the respective genes were selected for further analysis.

Exogenous BCOR Expression

HA-tagged BCOR-PUFD and CT domain cDNA was synthesized by Twist Bioscience. PUFD-, CT-, and 3× FLAG-tagged full-length BCOR cDNA was cloned into pXL303 plasmids (Addgene #25897) and packaged into lentiviral vectors using HEK293T cells. WT and BCOR/BCORL1 double-knockout K562 cells were transduced as described above.

In Vitro *Competition Assay*

Cas9-expressing K562 cells were transduced with a lentiviral vector expressing BFP or RFP657 fluorophores and sgRNAs targeting *BCOR*, *BCORL1*, *BCOR*, and *BCORL1*, *KDM2B*, or control. Cells expressing control or competitor sgRNAs were mixed in a 5:1 ratio and treated with either 0.01% DMSO, 1 μmol/L imatinib (Cell Signaling Technology), 1 μmol/L PD173074 (StemCell Technologies), or 1 μmol/L imatinib/PD173074, with or without 10 ng/mL FGF2 (Cell Signaling Technology) supplementation. Every 48 to 72 hours, cells were analyzed by flow cytometry using LSRFortessa (BD) and cell cultures were replenished with fresh medium. Diva software was used for data acquisition and FlowJo v10 for data analysis.

Cell Viability

Cells (2×10^4) were seeded in 50 μL media per well in a 96-well flat-bottom plate. Media were supplemented with 10 ng/mL FGF2. DMSO or FGFR inhibitor (PD173074) was added in limiting dilutions to the wells. Cell viability was analyzed after 72 hours using CellTiter-Glo Luminescence Cell Viability Assay (Promega). Cell viability was calculated relative to DMSO control.

Co-IP

For nuclear protein extraction, cells were washed with cold PBS and resuspended in cold Buffer A [10 mmol/L HEPES, 10 mmol/L KCl, 0.1 mmol/L EDTA, 0.1 mmol/L EGTA, 1× protease inhibitor cocktail (Thermo Fisher Scientific)]. Cells were allowed to swell on ice for 15 minutes before 10% IGEPAL (Sigma-Aldrich) was added. Lysates were pelleted at 14,000 rpm at 4°C for 5 minutes. Nuclei were washed with cold PBS and dissolved in modified RIPA buffer [0.1% IGEPAL, 0.1% sodium deoxycholate, 150 mmol/L NaCL, 50 mmol/L Tris pH 7.5, 1 U/μL Benzonase (MilliporeSigma), 1 mmol/L MgCl2, 2× protease inhibitor cocktail (Thermo Fisher Scientific)] at 4°C for 30 minutes with shaking. Cell debris was removed by centrifugation at 14,000 rpm at 4°C for 15 minutes. Protein concentrations in supernatants were quantified using the BCA assay kit (Thermo Fisher Scientific). A total of 1 mg nuclear extracts, 3.6 μg primary antibody or IgG control, and Dynabeads Protein G (Invitrogen) were incubated overnight at 4°C with shaking. Beads were washed three times with wash buffer (150 nmol/L NaCl, 50 mmol/L Tris pH 7.5) supplemented with 1% IGEPAL and three times with wash buffer only. Beads were eluted with LDS sample buffer (Bio-Rad Laboratories). The following antibodies were used for IP: BCOR (Proteintech, catalog no. 12107-1-AP, RRID:AB_2290335), BCORL1 (Bardwell Lab, RRID:AB_2889363), PCGF1 (Bardwell Lab, RRID:AB_2716801), KDM2B (Millipore, catalog no. 09-864, RRID:AB_10806072), HA (Abcam, catalog no. ab9110, RRID:AB_307019).

Western Blotting

For whole-cell lysates, cell pellets were resuspended in SDS loading buffer (Bio-Rad Laboratories). Nuclear extracts were prepared as described above. Cell lysates were separated on 4% to 12% SDS-PAGE gels and transferred to polyvinylidene difluoride membranes.

Membranes were blocked in 5% milk in TBST (1× Tris-buffered saline, 0.1% Tween 20 Detergent) for 1 hour at room temperature and incubated with primary antibody overnight at 4°C. Membranes were washed three times with TBST and incubated with secondary antibodies for 45 minutes at room temperature. Membranes were washed three times with TBST and incubated with SuperSignal West Dura or Femto substrate (Thermo Fisher Scientific) for 30 seconds. Images were captured using Bio-Rad ChemiDoc MP. Membranes were stripped using Restore Plus Stripping buffer (Thermo Fisher Scientific).

The following antibodies were used for Western blotting: BCOR (Proteintech, catalog no. 12107-1-AP, RRID:AB_2290335, 1:1,500), BCOR (Santa Cruz Biotechnology, catalog no. sc-514576, RRID:AB_2721913, 1:100), BCOR (Bardwell Lab, RRID:AB_2716801, 1:2,500), BCORL1 (Bardwell Lab, RRID:AB_2889363, 1:5,000), PCGF1 (Santa Cruz Biotechnology, catalog no. sc-515371, RRID:AB_2721914, 1:200), KDM2B (Millipore, catalog no. 09-864, RRID:AB_10806072, 1:1,000), RING1 (Abcam, catalog no. ab32644, AB_2238272, 1:1,000), RING1B/RNF2 (Santa Cruz Biotechnology, catalog no. sc-101109, RRID:AB_1129072, 1:200), H2AK119ub (Cell Signaling Technology, catalog no. 8240, RRID:AB_10891618, 1:3,000), H3K27me3 (Cell Signaling Technology, catalog no. 9733, RRID:AB_2616029, 1:1,000), BMI1 (Santa Cruz Biotechnology, catalog no. sc-390443, 1:200), PCGF3 (Thermo Fisher Scientific, catalog no. PA5-96686, RRID:AB_2808488, 1:1,000), PCGF5 (Abcam, catalog no. ab201511, 1:1,000), RYBP (Sigma-Aldrich, catalog no. PRS2227, RRID:AB_1847589, 1:1,000), CBX8 (Santa Cruz Biotechnology, catalog no. sc-374332, RRID:AB_10990104, 1:1,000), SKP1 (Abcam, catalog no. ab76502, RRID:AB_1524396, 1:1,000), HAUSP/USP7 (Abcam, catalog no. ab4080, RRID:AB_2214019, 1:1,000), HA-tag (Abcam, catalog no. ab9110, RRID:AB_307019, 1:5,000), FGFR1 (Cell Signaling Technology, catalog no. 9740S, RRID:AB_11178519, 1:1,000), β-Actin (Abcam, catalog no. ab20272, RRID:AB_445482, 1:10,000), and LMNB1/Lamin B1 (Abcam, catalog no. ab133741, RRID:AB_2616597, 1:10,000).

MS

On-bead Digest. IP was performed using 1 mg input protein (nuclear extract) and 3.6 μg BCOR antibody (RRID:AB_2290335) or 3.6 μg IgG (RRID:AB_1031062) as described above. Rep1 and Rep2 samples were processed and analyzed independently on 2 consecutive days. Samples were lysed in modified RIPA buffer [0.1% IGEPAL, 0.1% sodium deoxycholate, 150 mmol/L NaCL, 50 mmol/L Tris pH 7.5, 1 U/μL Benzonase (MilliporeSigma)]. Beads were washed three times with wash buffer (150 nmol/L NaCl, 50 mmol/L Tris pH 7.5) supplemented with 1% IGEPAL and three times with wash buffer only. The beads were resuspended in 20 μL of wash buffer, followed by 90 μL digestion buffer (2 mol/L urea, 50 mmol/L Tris HCl) and then 2 μg sequencing grade trypsin was added, followed by 1 hour of shaking at 700 rpm. The supernatant was removed and placed in a fresh tube. The beads were washed twice with 50 μL digestion buffer and combined with the supernatant. The combined supernatants were reduced (2 μL 500 mmol/L dithiothreitol, 30 minutes, room temperature) and alkylated (4 μL 500 mmol/L iodoacetamide, 45 minutes, dark), and a longer overnight digestion was performed: 2 μg (4 μL) trypsin and shaken overnight. The samples were then quenched with 20 μL 10% formic acid and desalted on 10-mg Oasis cartridges.

TMT Labeling of Peptides and Basic Reverse-Phase Fractionation. Desalted peptides from each sample in each replicate were labeled with TMT reagents (Pierce/Thermo Fisher Scientific). Peptides were dissolved in 30 μL of 50 mmol/L TEAB pH 8.5 solution (Sigma-Aldrich), and labeling reagent was added in 70 μL ethanol. After 1-hour incubation, the reaction was stopped with 50 mmol/L Tris/HCl pH 7.5. Differentially labeled peptides were mixed and subsequently desalted on 10-mg Oasis cartridges according to the following protocol: Cartridges were prepared for desalting by equilibrating with methanol, 50% ACN, and 1% formic acid and three washes with 0.1% TFA. Desalted peptides were then labeled individually with TMT10 reagent according to the manufacturer's instructions (Thermo Fisher Scientific).

For labeling with TMT, peptides from samples in each replicate were dissolved in 25 μL of 50 mmol/L HEPES pH 8.5 and 0.2 mg of TMT labeling reagent was added to each sample in 10 μL of CAN as follows: channel 126: WT_IgG; channel 127N: WT_BCOR-IP; channel 127C: BCORKO_IgG; channel 128N: BCORKO_BCOR-IP; channel 128C: PCGF1KO_IgG; channel 130N: PCGF1KO_BCOR-IP; channel 129C: BCORMUT_IgG (data not used in this article); and channel 129N: BCORMUT_BCOR-IP (data not used in this article). Samples were incubated with labeling reagent for 1 hour with agitation. Next, the reaction was quenched with 2 μL of 5% hydroxylamine. Differentially labeled peptides were subsequently mixed, and the combined samples were fractionated into six fractions using basic reverse-phase chromatography on Oasis Cartridges. Samples were loaded onto the cartridge and washed three times with 1% formic acid. A pH switch was performed with 5 mmol/L ammonium formate at pH 10, collected, and run as fraction 1. Subsequent fractions were collected at the following ACN concentrations: 10% ACN in 5 mmol/L ammonium formate; 20% ACN in 5 mmol/L ammonium formate; 30% CAN in 5 mmol/L ammonium formate; 40% ACN in 5 mmol/L ammonium formate; and 50% ACN in 5 mmol/L ammonium formate.

MS Analysis. Reconstituted peptides were separated on an online nanoflow EASY-nLC 1000 UHPLC system (Thermo Fisher Scientific) and analyzed on a benchtop Orbitrap Q Exactive Plus mass spectrometer (Thermo Fisher Scientific). The peptide samples were injected onto a capillary column (Picofrit with 10 μmol/L tip opening/75 μmol/L diameter, New Objective, PF360-75-10-N-5) packed in-house with 20 cm C18 silica material (1.9 μmol/L ReproSil-Pur C18-AQ medium, Maisch GmbH, r119.aq). The UHPLC setup was connected with a custom-fit microadapting tee (360 μmol/L, IDEX Health & Science, UH-753), and capillary columns were heated to 50°C in column heater sleeves (Phoenix-ST) to reduce backpressure during UHPLC separation. Injected peptides were separated at a flow rate of 200 nL/minute with a linear 80-minute gradient from 100% solvent A (3% acetonitrile, 0.1% formic acid) to 30% solvent B (90% acetonitrile, 0.1% formic acid), followed by a linear 6-minute gradient from 30% solvent B to 90% solvent B. Each sample was run for 120 minutes, including sample loading and column equilibration times. The Q Exactive Plus instrument was operated in the data-dependent mode acquiring higher energy collisional dissociation (HCD) MS-MS scans (R = 17,500) after each MS1 scan (R = 70,000) on the 12 most abundant ions using an MS1 ion target of 3×10^6 ions and an MS2 target of 5×10^4 ions. The maximum ion time utilized for the MS-MS scans was 120 ms; the HCD-normalized collision energy was set to 27; the dynamic exclusion time was set to 20 seconds, and the peptide match and isotope exclusion functions were enabled.

Quantification and Identification of Peptides and Proteins. All mass spectra were processed using the Spectrum Mill software package v.6.01 prerelease (Agilent Technologies), which includes modules developed for iTRAQ and TMT6-based quantification. Precursor ion quantification was done using extracted ion chromatograms for each precursor ion. The peak area for the extracted ion chromatogram of each precursor ion subjected to MS-MS was calculated in the intervening high-resolution MS1 scans of the LC/MS-MS runs using narrow windows around each individual member of the isotope cluster. Peak widths in both time and m/z domains were dynamically determined on the basis of MS scan resolution, precursor charge, and m/z, subject to quality metrics on the relative distribution of the peaks in the isotope cluster versus theoretical. Similar MS-MS spectra acquired on the same precursor m/z in the same dissociation

mode with ±60 seconds were merged. MS-MS spectra with precursor charge >7 and poor-quality MS-MS spectra, which failed the quality filter by having a sequence tag length less than 1, were excluded from searching.

For peptide identification, MS-MS spectra were searched against the human UniProt database to which a set of common laboratory contaminant proteins was appended. Search parameters included ESI-QEXACTIVE-HCD scoring parameters, trypsin or Lys-c/trypsin enzyme specificity with a maximum of two missed cleavage, 40% minimum matched peak intensity, ±20 ppm precursor mass tolerance, ±20 ppm product mass tolerance, and carbamidomethylation of cysteines and TMT-isobaric labeling of lysines and N-termini as fixed modifications. Oxidation of methionine, N-terminal acetylation, and deamidated (N) were allowed as variable modifications, with a precursor MH+ shift range from –18 to 64 Da. Identities interpreted for individual spectra were automatically designated as valid by optimizing score and delta rank1 to rank2 score thresholds separately for each precursor charge state in each LC/MS-MS run while allowing a maximum target decoy–based FDR of 1.0% at the spectrum level.

In calculating scores at the protein level and reporting the identified proteins, redundancy is addressed in the following manner: The protein score is the sum of the scores of distinct peptides. A distinct peptide is the single highest scoring instance of a peptide detected through an MS-MS spectrum. MS-MS spectra for a particular peptide may have been recorded multiple times (i.e., from different precursor charge states, isolated from adjacent basic reverse-phase fractions, or modified by oxidation of methionine), but are still counted as a single distinct peptide. When a peptide sequence over eight residues long is contained in multiple protein entries in the sequence database, the proteins are grouped together and the highest scoring one and its accession number are reported. In some cases in which the protein sequences are grouped in this manner, there are distinct peptides that uniquely represent a lower scoring member of the group (isoforms or family members). Each of these instances spawns a subgroup, and multiple subgroups are reported and counted toward the total number of proteins identified. TMT ratios were obtained from the protein comparisons export table in Spectrum Mill. To obtain TMT protein ratios, the median was calculated over all of the distinct peptides assigned to a protein subgroup in each replicate. We required each protein to be detected with two or more unique peptides. To enable precise quantification, we limited our analysis to peptides that are uniquely assigned to a specific protein isoform or family member. For statistical analysis, we used the Limma package (41) in R (https://www.r-project.org/) to calculate multiple comparison adjusted *P* values using a moderated *t* test.

Proteomics Analysis and Visualization

Nonhuman proteins, proteins with less than two unique peptides, and proteins not present in the current Hugo Gene Nomenclature Committee (HGNC) database of protein-coding genes (https://www.genenames.org/cgi-bin/statistics) were removed from further analyses. Ratios of intensities between channels were median-normalized. Statistical analyses were performed using a two-sample moderated *t* test from the R package limma (41) to estimate *P* values for each protein, and FDR corrections were applied to account for multiple hypothesis testing. Figures were generated using the R package ggplot2 version 3.2.1 (42).

RNA Sequencing

Total RNA was extracted using RNeasy Plus Mini Kit (Qiagen) or HighPure RNA Isolation Kit (Roche). Libraries were prepared using Roche Kapa mRNA HyperPrep strand-specific sample preparation kits from 200 ng of purified total RNA on a Beckman Coulter Biomek i7. The dsDNA libraries were quantified by Qubit fluorometer, Agilent TapeStation 2200, and RT-qPCR using the Kapa Biosystems library quantification kit. Dual-indexed libraries were pooled in equimolar ratios and sequenced on an Illumina NextSeq-550 (single-end 75 bp) or a NovaSeq-6000 (50-bp read pairs).

ChIP-seq

For histone ChIP-seq, cells were cross-linked for 10 minutes with 1% formaldehyde at room temperature on a shaker at 850 rpm. Cross-linked nuclei were quenched with 0.125 mol/L glycine for 5 minutes at room temperature and washed with PBS [containing protease inhibitor (Roche) and the histone deacetylase inhibitor sodium butyrate (NaBut)]. For ChIP-seq of BCOR, BCORL1, RNF2, KDM2B, and SUZ12, cells were first fixed with 2 mmol/L DSG (Thermo Fisher Scientific) for 45 minutes at room temperature, followed by formaldehyde cross-linking as described above. After fixation, pellets were resuspended in 500 µL of 1% SDS (50 mmol/L Tris-HCl pH 8, 10 mmol/L EDTA) and sonicated in 1 mL AFA fiber millitubes for 25 minutes using a Covaris E220 instrument (setting: 75 peak incident power, 5% duty factor, and 200 cycles per burst). Chromatin was immunoprecipitated using primary antibody and Dynabeads Protein A/G (Invitrogen). ChIP-seq libraries were made using the ThruPLEX DNA-seq 48D Rubicon kit and purified. A total of 75-bp single-end reads were sequenced on an Illumina NextSeq.

The following antibodies were used for ChIP-seq: BCOR (Proteintech, catalog no. 12107-1-AP, RRID:AB_2290335), BCORL1 (Bardwell Lab, RRID:AB_2889363), KDM2B (Millipore, catalog no. 17-10264, RRID:AB_11205420), RING1B/RNF2 (Cell Signaling Technology, catalog no. 5694S, RRID:AB_10705604), SUZ12 (Abcam, catalog no. ab12073, RRID:AB_442939), H2AK119ub (Cell Signaling Technology, catalog no. 8240, RRID:AB_10891618), H3K27me3 (Cell Signaling Technology, catalog no. 9733, RRID:AB_2616029), and H3K27ac (Diagenode, catalog no. C15410196, RRID:AB_2637079).

ATAC-seq

ATAC-seq experiments were performed using an adjusted version of the Omni-ATAC protocol (43). A total of 100,000 cells were resuspended in 50 µL cold ATAC-resuspension buffer (RSB; 10 mmol/L Tris-HCl pH 7.4, 10 mmol/L NaCl, and 3 mmol/L $MgCl_2$ in water) containing 0.1% NP40, 0.1% Tween-20, and 0.01% Digitonin and incubated on ice for 3 minutes. After lysis, 1 mL ATAC-RSB containing 0.1% Tween-20 was added to the mixture and centrifuged for 10 minutes at 1,500 RCF in a prechilled (4°C) fixed-angle centrifuge. Supernatant was removed and nuclei were resuspended in 50 µL transposition mix [2.5 µL transposase Tn5 (100 nmol/L final), 25 µL 2× TD buffer, 16.5 µL 1× PBS, 0.5 µL 1% Digitonin, 0.5 µL 10% Tween-20 in wate; ref. 43]. Transposition reactions were incubated at 37°C for 30 minutes in a thermomixer. Libraries were made as described previously (44). A total of 35-bp paired-end reads were sequenced on an Illumina NextSeq500.

Multiplexed Enhanced Reduced Representation Bisulfite Sequencing

DNA from K562 cells ($n = 3$) was extracted using the DNA Isolation Kit for Cells and Tissues from Roche (catalog no. 118147700011). Multiplexed enhanced reduced representation bisulfite sequencing was performed as described previously (45). Libraries were sequenced on a NovaSeq 6000 with 100-bp single-end reads.

RNA Sequencing Data Analysis

Raw reads were mapped to the GRCh38 build of the human genome by STAR (46). Gene counts were obtained using featureCounts (47). Normalization and differential gene expression analysis were performed using the R package DESeq2 version 1.24.0 (48). Gene expression levels were represented as box plots using normalized DESeq2 counts. Genes with expression fold changes greater than

2 and adjusted *P* values less than 0.05 were considered differentially expressed. GSEA was carried out using the gseKEGG function from clusterProfiler version 3.12.0 (P_{adj} cutoff value = 0.05, minimum gene set size = 70; ref. 49). The g:GOSt function from g:Profiler version e99_eg46_p14_f0f4439 (50) was used to detect significantly enriched KEGG pathways of PRC1.1-responsive genes ($n = 632$; Supplementary Fig. S5B). For unsupervised hierarchical clustering analysis and heat map generation in Fig. 5E, the count data were transformed using variance stabilizing transformation and analyzed using the R pheatmap package version 1.0.12 with default settings (default distance measure: Euclidean distance).

Raw RNA-sequencing counts from the Beat AML study (29) were obtained from the authors via the Vizome portal (http://www.vizome.org/aml/). Only AML samples with available whole-exome sequencing data were used for further analysis. AML samples with gene fusions, relapse samples, as well as serial samples were excluded from the analysis (number of samples after filtering: $n = 238$). Normalization and differential gene expression analysis were performed using the R package DESeq2 version 1.24.0 (48).

ChIP-seq and ATAC-seq Data Analysis

Quality control and preprocessing of raw ChIP-seq and ATAC-seq data was performed using the ChiLin pipeline (51). Reads were mapped to the hg19 human reference genome with BWA version 0.7.8 (35). Mapped reads were indexed and sorted using samtools version 1.9 (36). Peaks were called with MACS2 version 2.1.1 (ref. 52; https://github.com/macs3-project/MACS) at *–q* 0.01. The –SPMR option was used to generate bedgraph and bigwig files normalized to 1 million reads. Coverage tracks of bigwig files were visualized using the Integrative Genomics Viewer (IGV; ref. 53). Peak annotations and genomic distributions of high-confidence peaks [$–\log_{10}(q$ value) >10] were determined using the R package ChIPSeeker version 1.20.0 (54).

To determine ChIP or ATAC enrichment at promoter regions, the average signal score was calculated at TSS ± 5 kb using multiBigwigSummary from deepTools version 3.0.0 (ref. 55; with BED file and –outRawCounts options). Bigwig files normalized per million of mapped reads were used as input files.

Gene promoters with BCOR signal scores >0.1 in K562 WT cells were defined as PRC1.1-bound (n = 11,934; Fig. 4A). We included all canonical protein-coding transcripts in the genome from which we had gene expression data for this analysis (n = 18,573). H3K27ac signal scores in K562 WT cells were used to subdivide PRC1.1-bound genes into active (H3K27ac >0.1) or repressed (H3K27ac <0.1) genes (Fig. 5A; Supplementary Fig. S4A). PRC1.1-unbound gene promoters ($n = 6,639$) with H3K27ac signal scores <0.1 were classified as inactive (n = 6,269). PRC1.1-unbound gene promoters with H3K27ac signal scores >0.1 ($n = 370$) were not included in the analysis. We used the same approach to define active, repressed, and inactive chromatin states in $BCOR^{WT}$ primary AML cells (Supplementary Fig. S4D). For correlation analysis of BCOR- and BCORL1-ChIP-seq datasets, average signal scores at TSS ± 5 kb were calculated using multiBigwigSummary and plotted as pairwise scatter plots (Fig. 4B; Supplementary Fig. S3B).

For box plot representations in Fig. 5H, multiBigwigSummary signal scores at PRC1.1-responsive genes ($n = 632$) were shown relative to the signal scores at PRC1.1-nonresponsive genes (n = 1,799).

Heat maps and average density profiles of ChIP- or ATAC-signal enrichment at promoter regions were generated using computeMatrix (reference-point –referencePoint TSS -a 5000 -a 5000 -bs 50), followed by plotHeatmap or plotProfile from deepTools (55). Bigwig files normalized per million of mapped reads were used as input files. The option –regionsFileName was used to plot predefined regions. CpG-rich promoters (n = 10,851) and CpG-poor promoters (n = 7,352) were defined on the basis of CGI data from the UCSC Genome Browser version 2009–03–08 (56).

DNA Methylation Data Analysis

Sequencing reads were aligned against a bisulfite-converted human genome (hg19) using Bowtie version 1.2.2 (57), Bismark version 0.4.1 (58), and cutadapt (59) and the following code: /path/amp-errbs/ –prefix = myprefix –indir = /input_dir/ –illumina = 1.9 –adapter = NNAGATCGGAAGAGCACACGTCTGAACTCCAGTCAC –cutadapt –genomePath = /path/hg19chromFa. The function "tiling window analysis" from the R package methylKit version 1.10.0 (60) was used to summarize methylation information within 200-bp tiles. Methylation call files were then transformed to bed files for visualization using the IGV. The methylation status was represented with an 11-color gradient. Genomic coordinates, length, and CpG counts of CGIs were obtained from the CGI track from genome.ucsc.edu version 2009-03-08. Promoter regions (TSS ±250 bp) that overlapped with CGIs were determined with the BEDOPS closest-features function version 2.4.30 (61) and classified as CGI promoters (n = 10,851).

Quantification and Statistical Analysis

Data are represented as mean ± SD or mean ± SEM as indicated in the figure legends. Statistical parameters, including statistical significance and number of replicates, are described in the figure legends and in the Methods section. Statistical analyses were performed with GraphPad Prism software 8.4.3 (GraphPad Software).

Data Availability

All materials in this analysis are available upon request and Material Transfer Agreement from the corresponding author. The ChIP-seq, RNA-seq, ATAC-seq data reported in this article are available in the Gene Expression Omnibus under the accession number GSE167869.

Authors' Disclosures

E.J. Schaefer reports grants from the German Research Foundation (DFG) and Research School for Translational Medicine Goettingen (TRANSMED) during the conduct of the study. I. Fares reports grants from Canadian Institutes of Health Research (CIHR)-Banting Postdoctoral Fellowship during the conduct of the study. E.S. Winer reports other support from Pfizer, Jazz Pharmaceuticals, Curis, and Takeda outside the submitted work. J.S. Garcia reports nonfinancial support and other support from AbbVie; nonfinancial support from Genentech; personal fees from Astellas; and other support from Prelude, AstraZeneca, and Pfizer outside the submitted work. R.M. Stone reports personal fees from AbbVie, AbbVie/Genentech, Actinium, Amgen, Aprea, Astellas, Biolinerx, BerGenBio, Bristol Myers Squibb, Boston Pharmaceuticals, CTI Pharma, Daiichi Sankyo, Elevate Bio, Foghorn, Gemoab, GlaxoSmithKline, Innate, Janssen, Jazz, Macrogenics, OncoNova, Syros, Takeda, and Trovagene; personal fees and other support from Arog and Novartis; and other support from Celgene and Syntrix/ACI outside the submitted work. S.A. Carr is a scientific advisory board member for Kymera, PTMBio, and Seer. V.J. Bardwell reports grants from the NIH during the conduct of the study. M.E. Figueroa reports grants from the Leukemia & Lymphoma Society during the conduct of the study. R.C. Lindsley reports grants from the Edward P. Evans Foundation and NIH during the conduct of the study, as well as personal fees from Takeda Pharmaceuticals and Bluebird Bio, and other support from Jazz Pharmaceuticals outside the submitted work. No disclosures were reported by the other authors.

Authors' Contributions

E.J. Schaefer: Conceptualization, formal analysis, funding acquisition, investigation, methodology, writing–original draft, writing–review and editing. **H.C. Wang:** Formal analysis, investigation, methodology, writing–review and editing. **H.Q. Karp:** Validation, investigation. **C.A. Meyer:** Supervision, writing–review and editing.

P. Cejas: Supervision, writing–review and editing. **M.D. Gearhart:** Resources, supervision, writing–review and editing. **E.R. Adelman:** Formal analysis, investigation, writing–review and editing. **I. Fares:** Methodology, writing–review and editing. **A. Apffel:** Formal analysis, investigation, writing–review and editing. **K. Lim:** Investigation, writing–review and editing. **Y. Xie:** Formal analysis, writing–review and editing. **C.J. Gibson:** Writing–review and editing. **M. Schenone:** Supervision, writing–review and editing. **H.M. Murdock:** Resources, writing–review and editing. **E.S. Wang:** Resources, writing–review and editing. **L.P. Gondek:** Resources, writing–review and editing. **M.P. Carroll:** Resources, writing–review and editing. **R.S. Vedula:** Resources, writing–review and editing. **E.S. Winer:** Resources, writing–review and editing. **J.S. Garcia:** Resources, writing–review and editing. **R.M. Stone:** Resources, supervision, writing–review and editing. **M.R. Luskin:** Resources, writing–review and editing. **S.A. Carr:** Supervision, writing–review and editing. **H.W. Long:** Supervision, writing–review and editing. **V.J. Bardwell:** Resources, supervision, writing–review and editing. **M.E. Figueroa:** Supervision, writing–review and editing. **R.C. Lindsley:** Conceptualization, formal analysis, supervision, funding acquisition, writing–original draft, writing–review and editing.

Acknowledgments

This work was supported by the NIH [K08CA204734 (R.C. Lindsley) and R01HD084459 (V.J. Bardwell)], the Edward P. Evans Foundation (R.C. Lindsley), the German Research Foundation [DFG-SCHA2121/1-1 (E.J. Schaefer)], and the Research School for Translational Medicine Goettingen (E.J. Schaefer). This work was supported by the Dana-Farber Cancer Institute Center for Functional Cancer Epigenetics, the Ted and Eileen Pasquarello Tissue Bank in Hematologic Malignancies, and the Dana-Farber Cancer Institute Hematologic Malignancies Data Repository.

Received July 10, 2021; revised November 6, 2021; accepted December 10, 2021; published first December 17, 2021.

REFERENCES

1. Comet I, Riising EM, Leblanc B, Helin K. Maintaining cell identity: PRC2-mediated regulation of transcription and cancer. Nat Rev Cancer 2016;16:803–10.
2. Gao Z, Zhang J, Bonasio R, Strino F, Sawai A, Parisi F, et al. PCGF Homologs, CBX proteins, and RYBP define functionally distinct PRC1 family complexes. Mol Cell 2012;45:344–56.
3. Scelfo A, Fernández-Pérez D, Tamburri S, Zanotti M, Lavarone E, Soldi M, et al. Functional landscape of PCGF proteins reveals both RING1A/B-dependent-and RING1A/B-independent-specific activities. Mol Cell 2019;74:1037–52.
4. Gearhart MD, Corcoran CM, Wamstad JA, Bardwell VJ. Polycomb group and SCF ubiquitin ligases are found in a novel BCOR complex that is recruited to BCL6 targets. Mol Cell Biol 2006;26:6880–9.
5. Grossmann V, Tiacci E, Holmes AB, Kohlmann A, Martelli MP, Kern W, et al. Whole-exome sequencing identifies somatic mutations of BCOR in acute myeloid leukemia with normal karyotype. Blood 2011;118:6153–63.
6. Damm F, Chesnais V, Nagata Y, Yoshida K, Scourzic L, Itzykson R, et al. BCOR and BCORL1 mutations in myelodysplastic syndromes and related disorders. Blood 2013;122:3169–77.
7. Lindsley RC, Mar BG, Mazzola E, Grauman PV, Shareef S, Allen SL, et al. Acute myeloid leukemia ontogeny is defined by distinct somatic mutations. Blood 2015;125:1367–77.
8. Lindsley RC, Saber W, Mar BG, Redd R, Wang T, Haagenson MD, et al. Prognostic mutations in myelodysplastic syndrome after stem-cell transplantation. N Engl J Med 2017;376:536–47.
9. Papaemmanuil E, Gerstung M, Bullinger L, Gaidzik VI, Paschka P, Roberts ND, et al. Genomic classification and prognosis in acute myeloid leukemia. N Engl J Med 2016;374:2209–21.
10. Branford S, Wang P, Yeung DT, Thomson D, Purins A, Wadham C, et al. Integrative genomic analysis reveals cancer-associated mutations at diagnosis of CML in patients with high-risk disease. Blood 2018;132:948–61.
11. Terada K, Yamaguchi H, Ueki T, Usuki K, Kobayashi Y, Tajika K, et al. Usefulness of BCOR gene mutation as a prognostic factor in acute myeloid leukemia with intermediate cytogenetic prognosis. Genes Chromosomes Cancer 2018;57:401–8.
12. Iacobucci I, Qu C, Varotto E, Janke LJ, Yang X, Seth A, et al. Modeling and targeting of erythroleukemia by hematopoietic genome editing. Blood 2021;137:1628–40.
13. Ghetu AF, Corcoran CM, Cerchietti L, Bardwell VJ, Melnick A, Privé GG. Structure of a BCOR corepressor peptide in complex with the BCL6 BTB domain dimer. Mol Cell 2008;29:384–91.
14. Srinivasan RS, de Erkenez AC, Hemenway CS. The mixed lineage leukemia fusion partner AF9 binds specific isoforms of the BCL-6 corepressor. Oncogene 2003;22:3395–406.
15. Schmidt CR, Achille NJ, Kuntimaddi A, Boulton AM, Leach BI, Zhang S, et al. BCOR binding to MLL-AF9 is essential for leukemia via altered EYA1, SIX, and MYC activity. Blood Cancer Discov 2020;1:162–77.
16. Sportoletti P, Sorcini D, Falini B. BCOR gene alterations in hematological diseases. Blood 2021;138:2455–68.
17. Junco SE, Wang R, Gaipa JC, Taylor AB, Schirf V, Gearhart MD, et al. Structure of the polycomb group protein PCGF1 in complex with BCOR reveals basis for binding selectivity of PCGF homologs. Structure 2013;21:665–71.
18. Hurtz C, Hatzi K, Cerchietti L, Braig M, Park E, Kim YM, et al. BCL6-mediated repression of p53 is critical for leukemia stem cell survival in chronic myeloid leukemia. J Exp Med 2011;208:2163–74.
19. Huynh KD, Fischle W, Verdin E, Bardwell VJ. BCoR, a novel corepressor involved in BCL-6 repression. Genes Dev 2000;14:1810–23.
20. Béguelin W, Teater M, Gearhart MD, Calvo Fernández MT, Goldstein RL, Cárdenas MG, et al. EZH2 and BCL6 cooperate to assemble CBX8-BCOR complex to repress bivalent promoters, mediate germinal center formation and lymphomagenesis. Cancer Cell 2016;30:197–213.
21. Hatzi K, Jiang Y, Huang C, Garrett-bakelman F, Micah D, Giannopoulou EG, et al. A hybrid mechanism of action for BCL6 in B-cells defined by formation of functionally distinct complexes at enhancers and promoters. Cell Rep 2013;4:578–88.
22. Wang Z, Gearhart MD, Lee YW, Kumar I, Ramazanov B, Zhang Y, et al. A non-canonical BCOR-PRC1.1 complex represses differentiation programs in human ESCs. Cell Stem Cell 2018;22:235–51.
23. Farcas AM, Blackledge NP, Sudbery I, Long HK, McGouran JF, Rose NR, et al. KDM2B links the polycomb repressive complex 1 (PRC1) to recognition of CpG islands. Elife 2012;1:e00205.
24. He J, Shen L, Wan M, Taranova O, Wu H, Zhang Y. Kdm2b maintains murine embryonic stem cell status by recruiting PRC1 complex to CpG islands of developmental genes. Nat Cell Biol 2013;15:373–84.
25. Wu X, Johansen JV, Helin K. Fbxl10/Kdm2b recruits polycomb repressive complex 1 to CpG islands and regulates H2A ubiquitylation. Mol Cell 2013;49:1134–46.
26. Blackledge NP, Fursova NA, Kelley JR, Huseyin MK, Feldmann A, Klose RJ. PRC1 catalytic activity is central to polycomb system function. Mol Cell 2020;77:857–74.
27. Fursova NA, Blackledge NP, Nakayama M, Ito S, Koseki Y, Farcas AM, et al. Synergy between variant PRC1 complexes defines polycomb-mediated gene repression. Mol Cell 2019;74:1020–36.
28. Tamburri S, Lavarone E, Fernández-Pérez D, Conway E, Zanotti M, Manganaro D, et al. Histone H2AK119 mono-ubiquitination is essential for polycomb-mediated transcriptional repression. Mol Cell 2020;77:840–56.
29. Tyner JW, Tognon CE, Bottomly D, Wilmot B, Kurtz SE, Savage SL, et al. Functional genomic landscape of acute myeloid leukaemia. Nature 2018;562:526–31.
30. Traer E, Javidi-Sharifi N, Agarwal A, Dunlap J, English I, Martinez J, et al. Ponatinib overcomes FGF2-mediated resistance in CML patients without kinase domain mutations. Blood 2014;123:1516–24.

31. Traer E, Martinez J, Javidi-Sharifi N, Agarwal A, Dunlap J, English I, et al. FGF2 from marrow microenvironment promotes resistance to FLT3 inhibitors in acute myeloid leukemia. Cancer Res 2016;76: 6471–82.
32. Javidi-Sharifi N, Martinez J, English I, Joshi SK, Scopim-Ribeiro R, Viola SK, et al. FGF2-FGFR1 signaling regulates release of leukemia-protective exosomes from bone marrow stromal cells. Elife 2019;8:e40033.
33. van den Boom V, Maat H, Geugien M, Rodríguez López A, Sotoca AM, Jaques J, et al. Non-canonical PRC1.1 targets active genes independent of H3K27me3 and is essential for leukemogenesis. Cell Rep 2016;14:332–46.
34. Kelly MJ, So J, Rogers AJ, Gregory G, Li J, Zethoven M, et al. Bcor loss perturbs myeloid differentiation and promotes leukaemogenesis. Nat Commun 2019;10:1347.
35. Li H, Durbin R. Fast and accurate short read alignment with Burrows-Wheeler transform. Bioinformatics 2009;25:1754–60.
36. Li H, Handsaker B, Wysoker A, Fennell T, Ruan J, Homer N, et al. The Sequence Alignment/Map format and SAMtools. Bioinformatics 2009;25:2078–9.
37. Koboldt DC, Zhang Q, Larson DE, Shen D, McLellan MD, Lin L, et al. VarScan 2: somatic mutation and copy number alteration discovery in cancer by exome sequencing. Genome Res 2012;22:568–76.
38. Ye K, Schulz MH, Long Q, Apweiler R, Ning Z. Pindel: a pattern growth approach to detect break points of large deletions and medium sized insertions from paired-end short reads. Bioinformatics 2009;25:2865–71.
39. Richardson CD, Ray GJ, DeWitt MA, Curie GL, Corn JE. Enhancing homology-directed genome editing by catalytically active and inactive CRISPR-Cas9 using asymmetric donor DNA. Nat Biotechnol 2016;34:339–44.
40. Brinkman EK, Chen T, Amendola M, Van Steensel B. Easy quantitative assessment of genome editing by sequence trace decomposition. Nucleic Acids Res 2014;42:e168.
41. Ritchie ME, Phipson B, Wu D, Hu Y, Law CW, Shi W, et al. limma powers differential expression analyses for RNA-sequencing and microarray studies. Nucleic Acids Res 2015;43:e47.
42. Wickham H. Getting started with ggplot2. In: Wickham H, editor. ggplot2: elegant graphics for data analysis. Cham (Switzerland): Springer International Publishing; 2016. p. 11–31.
43. Corces MR, Trevino AE, Hamilton EG, Greenside PG, Sinnott-Armstrong NA, Vesuna S, et al. An improved ATAC-seq protocol reduces background and enables interrogation of frozen tissues. Nat Methods 2017;14:959–62.
44. Buenrostro JD, Wu B, Chang HY, Greenleaf WJ. ATAC-seq: a method for assaying chromatin accessibility genome-wide. Curr Protoc Mol Biol 2015;109:21.29.1–9.
45. Garrett-Bakelman FE, Sheridan CK, Kacmarczyk TJ, Ishii J, Betel D, Alonso A, et al. Enhanced reduced representation bisulfite sequencing for assessment of DNA methylation at base pair resolution. J Vis Exp 2015;e52246.
46. Dobin A, Davis CA, Schlesinger F, Drenkow J, Zaleski C, Jha S, et al. STAR: ultrafast universal RNA-seq aligner. Bioinformatics 2013;29:15–21.
47. Liao Y, Smyth GK, Shi W. featureCounts: an efficient general purpose program for assigning sequence reads to genomic features. Bioinformatics 2014;30:923–30.
48. Love MI, Huber W, Anders S. Moderated estimation of fold change and dispersion for RNA-seq data with DESeq2. Genome Biol 2014;15:550.
49. Yu G, Wang LG, Han Y, He QY. clusterProfiler: an R package for comparing biological themes among gene clusters. OMICS 2012;16:284–7.
50. Raudvere U, Kolberg L, Kuzmin I, Arak T, Adler P, Peterson H, et al. g:Profiler: a web server for functional enrichment analysis and conversions of gene lists (2019 update). Nucleic Acids Res 2019;47:W191–8.
51. Qin Q, Mei S, Wu Q, Sun H, Li L, Taing L, et al. ChiLin: a comprehensive ChIP-seq and DNase-seq quality control and analysis pipeline. BMC Bioinformatics 2016;17:404.
52. Zhang Y, Liu T, Meyer CA, Eeckhoute J, Johnson DS, Bernstein BE, et al. Model-based analysis of ChIP-seq (MACS). Genome Biol 2008; 9:R137.
53. Robinson JT, Thorvaldsdóttir H, Winckler W, Guttman M, Lander ES, Getz G, et al. Integrative genomics viewer. Nat Biotechnol 2011;29: 24–6.
54. Yu G, Wang LG, He QY. ChIPseeker: an R/Bioconductor package for ChIP peak annotation, comparison and visualization. Bioinformatics 2015;31:2382–3.
55. Ramírez F, Ryan DP, Grüning B, Bhardwaj V, Kilpert F, Richter AS, et al. deepTools2: a next generation web server for deep-sequencing data analysis. Nucleic Acids Res 2016;44:W160–5.
56. Gardiner-Garden M, Frommer M. CpG islands in vertebrate genomes. J Mol Biol 1987;196:261–82.
57. Langmead B, Trapnell C, Pop M, Salzberg SL. Ultrafast and memory-efficient alignment of short DNA sequences to the human genome. Genome Biol 2009;10:R25.
58. Krueger F, Andrews SR. Bismark: a flexible aligner and methylation caller for Bisulfite-Seq applications. Bioinformatics 2011;27:1571–2.
59. Martin M. Cutadapt removes adapter sequences from high-throughput sequencing reads. EMBnet J 2011;17:10–2.
60. Akalin A, Kormaksson M, Li S, Garrett-Bakelman FE, Figueroa ME, Melnick A, et al. methylKit: a comprehensive R package for the analysis of genome-wide DNA methylation profiles. Genome Biol 2012;13:R87.
61. Neph S, Kuehn MS, Reynolds AP, Haugen E, Thurman RE, Johnson AK, et al. BEDOPS: high-performance genomic feature operations. Bioinformatics 2012;28:1919–20.
62. Altschul SF, Madden TL, Schäffer AA, Zhang J, Zhang Z, Miller W, et al. Gapped BLAST and PSI-BLAST: a new generation of protein database search programs. Nucleic Acids Res 1997;25:3389–402.
63. Corces MR, Buenrostro JD, Wu B, Greenside PG, Chan SM, Koenig JL, et al. Lineage-specific and single-cell chromatin accessibility charts human hematopoiesis and leukemia evolution. Nat Genet 2016;48:1193–203.